CCFE
CULHAM CENTRE FOR FUSION ENERGY

UK Atomic Energy Authority

UKAEA-CCFE-PR(18)22

L. Garzotti, P. Belo, G. Corrigan, D. Harting, F. Köchl, A. Loarte, E. Militello Asp, V. Parail, R. Ambrosino, M. Cavinato, M. Mattei, M. Romanelli, R. Sartori and M. Valovič

# Integrated core-SOL modelling of fuelling, density control and divertor heat loads for the flat-top phase of the ITER H-mode D-T scenario

# Integrated core-SOL modelling of fuelling, density control and divertor heat loads for the flat-top phase of the ITER H-mode D-T scenario

L. Garzotti,[1] P. Belo,[1] G. Corrigan,[1] D. Harting,[1] F. Köchl,[1] A. Loarte,[2] E. Militello Asp,[1] V. Parail,[1] R. Ambrosino,[3] M. Cavinato,[5] M. Mattei,[4] M. Romanelli,[1] R. Sartori[5] and M. Valovič[1]

*[1]Culham Science Centre, OX14 3DB Abingdon, United Kingdom*

*[2]ITER Organization, Route de Vinon sur Verdon, 13115 St Paul Lez Durance, France*

*[3]CREATE, University of Naples "Federico II", Italy*

*[4]CREATE, University of Campania "Luigi Vanvitelli", Italy*

*[5]Fusion For Energy Joint Undertaking, Josep Pla 2, 08019, Barcelona, Spain*

This is a preprint of a paper submitted for publication in Nuclear Fusion

# Integrated core-SOL modelling of fuelling, density control and divertor heat loads for the flat-top phase of the ITER H-mode D-T scenario

**L. Garzotti†, P. Belo†, G. Corrigan†, D. Harting†, F. Köchl†, A. Loarte‡, E. Militello Asp†, V. Parail†, R. Ambrosino§, M. Cavinato‖, M. Mattei¶, M. Romanelli†, R. Sartori‖, M. Valovič†**

† Culham Science Centre, OX14 3DB Abingdon, United Kingdom
‡ ITER Organization, Route de Vinon sur Verdon, 13115 St Paul Lez Durance, France
§ CREATE, University of Naples "Federico II", Italy
¶ CREATE, University of Campania "Luigi Vanvitelli", Italy
‖ Fusion For Energy Joint Undertaking, Josep Pla 2, 08019, Barcelona, Spain

**Abstract.** The operation of a tokamak designed to test the sustainability of a thermonuclear grade plasma like the International Tokamak Experimental Reactor (ITER) presents several challenges. Among them is the necessity of fuelling the plasma to reach the density required to generate enough fusion power to achieve $Q = 10$ and, at the same time, to protect the divertor from melting by keeping the power density flux impinging directly onto it below 10 MW $m^{-2}$. Whether this goal is achievable or not depends on the details of the fuelling scheme, of the atomic species that are injected into the plasma, of the power radiation pattern in the scrape-off layer and in the divertor, of the additional heating schemes and of the transport mechanisms at work in the core and near the edge of the plasma.

In this paper we present, for different operational scenarios, the results of an integrated modelling approach to the problem taking into account all the different aspects of it. The tool adopted for our simulation is the JINTRAC suite of codes, which can simulate in an integrated fashion the transport of particles and heat in different regions of the plasma.

We show that, by carefully tuning the gas fuelling and impurity seeding, it is indeed possible on ITER to achieve $Q = 10$ and at the same time maintain the divertor in a safe operational condition. We also investigate the sensitivity of this result to the uncertainties in the modelling assumptions underlying the simulations presented in the paper.

PACS numbers: 52.55.Fa, 52.55.-s, 52.65.-y, 52.25.Fi, 28.52.Cx

## 1. Introduction

The fuelling and the control of the plasma density in ITER present many challenges and uncertainties. The high density and temperature at the separatrix will almost certainly make the scrape-off layer (SOL) opaque to the neutral penetration and the fuelling by means of gas puff less efficient than in present-day experiments. Therefore, depending on the transport characteristics of the SOL and the pedestal, other methods like, for example, pellet injection will probably be needed to reach the density required during the different phases of the discharge. In addition, the power flowing through the SOL will have to be reduced in order to avoid damaging the divertor plates but, at the same time, be high enough to maintain partial attachment and avoid the onset of thermal instabilities like a MARFE (multifaceted asymmetric radiation from the edge). To model this problem comprehensively and self-consistently, it is necessary to take an integrated approach including the description of the core plasma, the SOL and the interaction with the first wall and the divertor plates. These simulations have been the focus of a modelling activity carried on within the framework of a Fusion for Energy grant (GRT502) and some general results regarding different phases of an ITER baseline pulse (L-mode, current ramp-up, L-H transition, H-mode, H-L transition and current ramp-down and termination) have been reported in [1] and [2] both for the non-active (H and He) and active (D and D-T) phase of ITER operations.

In this paper we build on previous results, but we concentrate on the flat-top of a D-T H-mode ITER plasma and present the results of detailed fully integrated core-SOL simulations of fuelling and density control at different currents, fields and levels of additional power. The material is organized as follows: in section 2 we describe the main modelling assumptions underlying the study, in section 3, 4, 5 and 6 we present the results at 5 MA, 7.5 MA, 10 MA and 15 MA respectively (including scans performed to address particular aspects of the physics involved and to test the sensitivity of the results to the modelling assumptions), in section 7 we discuss the results obtained in the simulations and in section 8 we summarize the main conclusions of the work including the sensitivity to parameters affected by significant uncertainty.

## 2. Description of the simulations

The simulations presented in this study were performed with the JINTRAC suite of codes developed at JET [3], which allows to run JETTO/SANCO (for main ion and impurity core transport), EDGE2D (for main ion and impurity SOL transport) and EIRENE (neutral transport) in a coupled fashion. In our simulations the core transport is split between neoclassical and anomalous. The neoclassical transport for main gas and impurities is given by NCLASS [4], whereas the anomalous transport is calculated with the Bohm/gyro-Bohm transport model [5]. This choice was dictated by the relatively low computational burden and the excellent numerical stability of the Bohm/gyro-Bohm transport model. However, to take into account a collisionality-dependent inward particle pinch present in more advanced physics based models, like, for example, GLF23 [6], the Bohm/gyro-Bohm model was modified with the addition of a convective velocity $v_{inw}$ of the form $v_{inw}(\nu^*) = f(\nu^*)\, 0.5\, D\, r/a^2$ where $D$ is the cross-field particle diffusivity, $\nu^*$ is the normalized electron collisionality and $f(\nu^*) = \min(1, \exp(1 - \nu^*/\nu_{th}))$. We fitted the constant $\nu_{th} = 0.04$ by matching the density profiles obtained in Bohm/gyro-Bohm transport simulations for ITER at different current and field with the density profiles obtained in GLF23 transport

simulations in identical conditions.

The transport in the edge transport barrier (ETB) is treated by the continuous ELM model described in [7], which mimics the limiting effect of the ELMs on the pressure gradient in the ETB by introducing additional transport averaged over time and clamps the normalized pressure gradient in the ETB, $\alpha$, at a prescribed critical value, $\alpha_c$. The height and the width of the pedestal (and, therefore, $\alpha_c$) are estimated according to the EPED1 model [8] on the basis of peeling-ballooning stability and a proportionality between pedestal width and $\sqrt{\beta_p}$.

To describe the perpendicular transport in the scrape-off layer (SOL) we have assumed constant transport coefficients based on existing modelling of JET L-mode plasmas [9, 10]. Typical values used in this study are $D_{SOL} = 0.15$ m$^s$/s and $\chi_{SOL;i,e} = 0.5$ m$^2$/s. A sensitivity study of the simulation results to the details of the perpendicular transport in the SOL was conducted for the ITER L-mode and can be found in [11].

The particle sources considered in this study were neutral beam ionization, gas puff, wall recycling and pellet injection. The neutral beam particle source is calculated by the PENCIL code [12]. Gas puff and wall recycling are treated inside the Monte Carlo code EIRENE [13]. The pellet source can be treated in a simplified way by the continuous pellet model, whereby an additional time-averaged particle source with a Gaussian radial profile is introduced in the density transport equation. The centre and the width of the Gaussian, which approximate the pellet deposition profile, and the intensity of the source, which is linked to the pellet particle throughput, are prescribed as input parameters. It is clear that this simplified model does not capture the intermittent nature of pellet injection. A more realistic description of the pellet source is given by the ablation/deposition code HPI2, which treats simultaneously the evaporation of the pellet and the fast transport associated with the drift of the dense and cold plasmoid surrounding the pellet [14] and can be used to calculate an instantaneous (i. e. not time-averaged) particle source every time a pellet is injected in the plasma. The particle sink due to the pumps is modelled as a segment of the first wall located at the base of the divertor with albedo 0.97.

The heat sources associated with neutral beam injection (NBI) were calculated with PENCIL and the heat sources associated with ion and electron cyclotron resonance heating (ICRH and ECRH) were taken into account by prescribing fixed power deposition profiles obtained from stand alone calculations.

The composition of the core plasma was self-consistently calculated by the Bohm/gyro-Bohm transport model assuming a 50-50 D-T influx at the separatrix, with Be as main impurity coming from the first wall and Ne resulting from the seeding needed to radiate in the SOL part of the power crossing the separatrix and mitigate the divertor power load. In the SOL, however, because the version of EDGE2D used in this study was not able to simulate a two-species main plasma, we prescribed a pure D plasma with Be and Ne as impurities. The plasma facing materials were assumed to be Be for the wall and W for the divertor. However, it should be noted that some initial simulations reported here were obtained with a Be divertor. In any case, because of the computational burden imposed on the computation of the SOL dynamics the transport of W was not taken into account in the simulations presented in this paper.

**Table 1.** Main plasma parameters achievable for different fuelling and heating conditions in an ITER D-T H-mode plasma at 5 MA / 5.3 T. (Be divertor). $P_{NBI}$, $P_{ECRH}$ and $P_{ICRH}$ are the total NBI, ECRH and ICRH power respectively; $\Gamma_{D-T}$ and $\Gamma_{Ne}$ are the nominal main gas and Ne seeding throughput respectively; $f_G$ is the Greenwald fraction; $n_e(0)$ and $< n_e >$, $T_e(0)$ and $< T_e >$, $T_i(0)$ and $< T_i >$ are the on-axis and volume average electron density and electron and ion temperature respectively; $P_{fus}$ and $Q$ are the fusion power and the fusion gain respectively, $Z_{eff}$ is the effective charge and $P_{IT}$ and $P_{OT}$ are the peak power density on the inner and outer divertor target respectively. The same notation is used in all the tables in this paper.

| Case | A | B |
|---|---|---|
| $P_{NBI}$ / $P_{ECRH}$ / $P_{ICRH}$ [MW] | 33 / - / 20 | 33 / - / 20 |
| $\Gamma_{D-T}$ [$10^{22}$ s$^{-1}$] / $\Gamma_{Ne}$ [$10^{20}$ s$^{-1}$] | 0.5 / - | 1.0 / - |
| $f_G$ | 0.68 | 0.80 |
| $n_e(0)$ / $< n_e >$ [$10^{19}$ m$^{-3}$] | 3.3 / 2.7 | 4.0 / 3.2 |
| $T_e(0)$ / $< T_e >$ [keV] | 13.0 / 5.4 | 11.4 / 4.4 |
| $T_i(0)$ / $< T_i >$ [keV] | 15.8 / 5.5 | 12.0 / 4.2 |
| $P_{fus}$ [MW] / $Q$ | 15.3 / 0.29 | 17.9 / 0.34 |
| Divertor material | Be | Be |
| $Z_{eff}$ | 2.0 | 1.3 |
| $P_{IT}$ / $P_{OT}$ [MW m$^{-2}$] | 1.6 / 2.8 | 0.9 / 1.4 |

## 3. Results at 5MA

The fuelling of an ITER D-T baseline scenario at 5 MA, 5.3 T and 53 MW of additional power (33 MW NBI and 20 MW ICRH) was simulated at two different levels of gas puff: $0.5{\cdot}10^{22}$ s$^{-1}$ and $1.0{\cdot}10^{22}$ s$^{-1}$. Above this level of fuelling the simulations show a collapse of the temperature at the divertor target and the onset of a numerical instability in the code. This is an indication that the plasma is becoming detached and a thermal instability similar to a MARFE could be triggered. This is not surprising given that, for this relatively low plasma current, the fusion power and the power flux across the separatrix are too low to sustain an attached divertor. A summary of the results is given in table 1 where we show the main steady-state plasma parameters achievable under this fuelling and heating conditions. It is worth noting that, despite the limits on fuelling rate, the average density remains above the threshold for neutral beam shine-through loads on the first wall ($\sim$2.5-3.0$\cdot10^{19}$ m$^{-3}$), which ensures that the full NBI power of 33 MW and ion energy of 1 MeV can be used in ITER for these plasma conditions.

## 4. Results at 7.5 MA

For the scenario at 7.5 MA we performed five series of simulations: a fuelling rate scan at 5.3 T and 53 MW of additional power, a similar scan at 2.65 T and 53 MW of additional power, a third and fourth fuelling rate scans at 2.65 T and additional power reduced to 33 MW with both Be and W divertor and, finally, a fifth series of simulations at 2.65 T and 33 MW of additional power where gas fuelling was complemented with pellet injection.

**Table 2.** Main plasma parameters achievable for different fuelling and heating conditions in an ITER D-T H-mode plasma at 7.5 MA / 5.3 T and 53 MW of additional power.

| Case | A | B |
|---|---|---|
| $P_{NBI}$ / $P_{ECRH}$ / $P_{ICRH}$ [MW] | 33 / - / 20 | 33 / - / 20 |
| $\Gamma_{D-T}$ [$10^{22}$ s$^{-1}$] / $\Gamma_{Ne}$ [$10^{20}$ s$^{-1}$] | 0.5 / - | 1.0 / - |
| $f_G$ | 0.58 | 0.65 |
| $n_e(0)$ / $< n_e >$ [$10^{19}$ m$^{-3}$] | 4.3 / 3.4 | 4.8 / 3.8 |
| $T_e(0)$ / $< T_e >$ [keV] | 15.2 / 7.2 | 14.3 / 6.6 |
| $T_i(0)$ / $< T_i >$ [keV] | 18.0 / 7.3 | 16.0 / 6.5 |
| $P_{fus}$ [MW] / $Q$ | 47.0 / 0.89 | 51.3 / 0.97 |
| Divertor material | Be | Be |
| $Z_{eff}$ | 1.6 | 1.4 |
| $P_{IT}$ / $P_{OT}$ [MW m$^{-2}$] | 2.0 / 3.7 | 1.5 / 2.4 |

**Table 3.** Main plasma parameters achievable for different fuelling and heating conditions in an ITER D-T H-mode plasma at 7.5 MA / 2.65 T and 53 MW of additional power.

| Case | A | B | C | D |
|---|---|---|---|---|
| $P_{NBI}$ / $P_{ECRH}$ / $P_{ICRH}$ [MW] | 33 / - / 20 | 33 / - / 20 | 33 / - / 20 | 33 / - / 20 |
| $\Gamma_{D-T}$ [$10^{22}$ s$^{-1}$] / $\Gamma_{Ne}$ [$10^{20}$ s$^{-1}$] | 0.5 / - | 1.0 / - | 1.5 / - | 2.0 / - |
| $f_G$ | 0.48 | 0.60 | 0.66 | 0.68 |
| $n_e(0)$ / $< n_e >$ [$10^{19}$ m$^{-3}$] | 3.4 / 2.8 | 4.3 / 3.5 | 4.8 / 3.9 | 5.0 / 4.0 |
| $T_e(0)$ / $< T_e >$ [keV] | 13.0 / 7.6 | 11.5 / 6.4 | 10.8 / 5.9 | 10.5 / 5.7 |
| $T_i(0)$ / $< T_i >$ [keV] | 16.0 / 8.0 | 12.8 / 6.4 | 11.7 / 5.8 | 11.3 / 5.6 |
| $P_{fus}$ [MW] / $Q$ | 34.9 / 0.66 | 38.5 / 0.73 | 39.3 / 0.74 | 39.8 / 0.75 |
| Divertor material | Be | Be | Be | Be |
| $Z_{eff}$ | 1.6 | 1.4 | 1.3 | 1.3 |
| $P_{IT}$ / $P_{OT}$ [MW m$^{-2}$] | 3.9 / 6.1 | 2.9 / 4.6 | 2.5 / 3.3 | 2.6 / 2.7 |

### *4.1. Results at 7.5 MA / 5.3 T / 53 MW and 7.5 MA / 2.65 T / 53 MW.*

The results of the simulations at 7.5 MA and 53 MW of additional heating power are summarized in tables 2 and 3 and show that, for fuelling rates up to $1.0{\cdot}10^{22}$ s$^{-1}$, at 5.3 T one can reach a higher core temperature than at 2.65 T, because of a reduced sawtooth activity and a higher density for the same fuelling rate, due to a higher separatrix density. However, because the SOL heat flux width is larger at 5.3 T than at 2.65 T (due to the longer connection length), this leads to lower SOL power densities and an earlier onset of detachment at lower fuelling rates for 5.3 T than for 2.65 T. As a consequence, higher plasma densities are reached at 2.65 T at higher fuelling rates (up to $2.0{\cdot}10^{22}$ s$^{-1}$).

**Table 4.** Main plasma parameters achievable for different fuelling and heating conditions in an ITER D-T H-mode plasma at 7.5 MA / 2.65 T and 33 MW of additional power. (Be divertor).

| Case | A | B | C | D |
|---|---|---|---|---|
| $P_{NBI}$ / $P_{ECRH}$ / $P_{ICRH}$ [MW] | 33 / - / - | 33 / - / - | 33 / - / - | 33 / - / - |
| $\Gamma_{D-T}$ [$10^{22}$ s$^{-1}$] / $\Gamma_{Ne}$ [$10^{20}$ s$^{-1}$] | 0.5 / - | 1.0 / - | 1.5 / - | 2.0 / - |
| $f_G$ | 0.43 | 0.55 | 0.60 | 0.65 |
| $n_e(0)$ / $< n_e >$ [$10^{19}$ m$^{-3}$] | 3.2 / 2.5 | 4.0 / 3.2 | 4.4 / 3.5 | 4.7 / 3.8 |
| $T_e(0)$ / $< T_e >$ [keV] | 11.1 / 7.0 | 9.7 / 5.9 | 9.3 / 5.5 | 8.9 / 5.2 |
| $T_i(0)$ / $< T_i >$ [keV] | 9.8 / 6.2 | 8.6 / 5.3 | 8.2 / 5.0 | 7.8 / 4.7 |
| $P_{fus}$ [MW] / $Q$ | 21.6/ 0.65 | 22.3 / 0.68 | 22.2 / 0.67 | 22.2 / 0.67 |
| Divertor material | Be | Be | Be | Be |
| $Z_{eff}$ | 1.14 | 1.06 | 1.05 | 1.05 |
| $P_{IT}$ / $P_{OT}$ [MW m$^{-2}$] | 2.3 / 3.8 | 1.8 / 2.0 | 1.5 / 1.7 | 1.6 / 1.1 |

**Table 5.** Main plasma parameters achievable for different fuelling and heating conditions in an ITER D-T H-mode plasma at 7.5 MA / 2.65 T and 33 MW of additional power. (W divertor).

| Case | A | B | C | D |
|---|---|---|---|---|
| $P_{NBI}$ / $P_{ECRH}$ / $P_{ICRH}$ [MW] | 33 / - / - | 33 / - / - | 33 / - / - | 33 / - / - |
| $\Gamma_{D-T}$ [$10^{22}$ s$^{-1}$] / $\Gamma_{Ne}$ [$10^{20}$ s$^{-1}$] | 0.5 / - | 1.0 / - | 1.5 / - | 2.0 / - |
| $f_G$ | 0.43 | 0.56 | 0.63 | 0.67 |
| $n_e(0)$ / $< n_e >$ [$10^{19}$ m$^{-3}$] | 3.2 / 2.5 | 4.2 / 3.3 | 4.6 / 3.7 | 4.9 / 3.9 |
| $T_e(0)$ / $< T_e >$ [keV] | 11.0 / 7.0 | 9.5 / 5.7 | 8.7 / 5.3 | 8.5 / 5.0 |
| $T_i(0)$ / $< T_i >$ [keV] | 9.7 / 6.1 | 8.3 / 5.1 | 7.9 / 4.8 | 7.7 / 4.6 |
| $P_{fus}$ [MW] / $Q$ | 22.4/ 0.68 | 22.7 / 0.69 | 22.5 / 0.68 | 22.4 / 0.68 |
| Divertor material | W | W | W | W |
| $Z_{eff}$ | 1.00 | 1.00 | 1.00 | 1.02 |
| $P_{IT}$ / $P_{OT}$ [MW m$^{-2}$] | 2.3 / 6.7 | 1.8 / 2.6 | 1.6 / 1.9 | 1.7 / 1.2 |

### *4.2. Results at 7.5 MA / 2.65 T / 33 MW. Be and W divertor.*

The results obtained for a reduction in auxiliary power to 33 MW are summarized in tables 4 and 5 and are comparable to those with 53 MW. In these simulations, the ratio between the net power flowing through the separatrix and the L-H transition power threshold, $P_{net}/P_{L-H}$ is between 1.5 and 2.0, but the plasma remains deeply in H-mode. Core temperatures and densities are reduced by about 2 keV and $0.25{\cdot}10^{19}$ m$^{-3}$, due to the lower power input. The maximum gas puff rates allowed before the appearance of numerical problems indicating the occurrence of a thermal instability in the divertor is of the same order of magnitude as for the case with 53 MW of additional power. The plasma volume average density tends to saturate for $\Gamma_{D-T} \approx 2.0 \cdot 10^{22}$ s$^{-1}$. For higher gas puff rates, the onset of a numerical instability in the simulations indicates that the plasma starts to become detached. For low gas puff rates ($\Gamma_{D-T} \leq 1.0 \cdot 10^{22}$ s$^{-1}$), the ion temperature on the outer target is predicted to exceed the critical level for W sputtering of ∼5 eV in regions with significant ion

current density. Although core temperatures in the order of ∼10 keV can be obtained due to operation at low density, the fusion power remains ∼22 MW, giving $Q$ slightly below 0.7. The power flux across the separatrix $P_{sep}$ thus remains close to $P_{aux}$. Due to the low $P_{sep}$, the power density on the targets can be maintained well below 10 MW $m^{-2}$ without the need for Ne seeding, even for low gas fuelling rates. In cases with Be targets, $Z_{eff}$ is only marginally higher than in the cases with W targets. This seems to be due to operation at low power where Be sputtering at the target plates is much lower compared to the baseline scenario scans with Be targets at higher power, which will be presented in subsection 6.1. $Z_{eff}$ is also significantly lower compared to the same gas puff scan at 53 MW. This may explain why predicted edge densities do not deviate considerably for the cases with $P_{aux} = 33$ MW and $P_{aux} = 53$ MW. Higher $P_{sep}$ in case with $P_{aux} = 53$ MW seems to be partially compensated by increased impurity radiation in the SOL. Due to the small difference in impurity contamination, the results obtained with Be targets are quite similar to those obtained with W targets. Switching from Be to W targets, the core density is increased by a few percent only, whereas power densities and temperatures on the target plates are slightly increased as a consequence of reduced impurity radiation in the SOL.

### *4.3. Results at 7.5 MA / 2.65 T / 33 MW. Discrete pellets.*

To study the use of pellet fuelling on this ITER scenario, we started from a simulation of a 7.5 MA, 2.65 T plasma with 33 MW of additional heating power and $5.0 \cdot 10^{21}$ $s^{-1}$ D-T gas puff from the main chamber wall, which reached a steady-state volume average density of $3.4 \cdot 10^{19}$ $m^{-3}$. This simulation is similar to the one in the first column of table 4 except for the addition of a $1.0 \cdot 10^{20}$ $s^{-1}$ Ne gas puff from the divertor region. The reference simulation was continued for 2 s by introducing discrete pellets (mass $4.4 \cdot 10^{21}$ atoms, speed 300 m/s, composition 50-50 D-T) and prescribing a target volume-average density for the feed-back mechanism controlling the pellet injection of $4 \cdot 10^{19}$ $m^{-3}$ and $5 \cdot 10^{19}$ $m^{-3}$. The choice for these target volume-average densities was dictated by the fact that we wanted, on one side, to increase the Greenwald fraction from the continuous pellet case to a value equivalent to the 15 MA, 5.3 T plasma (i. e. $f_G \approx 0.85$) and, on the other side, to test an intermediate value between the continuous pellet case and the highest Greenwald fraction prescribed.

The background gas puff was maintained at $5.0 \cdot 10^{21}$ $s^{-1}$. For the scenario with target volume-average density $4 \cdot 10^{19}$ $m^{-3}$ a case was run with background gas puff at $1.0 \cdot 10^{21}$ $s^{-1}$ to test the effect on the divertor power load. The results are illustrated in figure 2, which shows that the target volume-average densities are easily achieved with the injection of five pellets in the case of $5 \cdot 10^{19}$ $m^{-3}$ target density and maintained with a pellet injection frequency of ∼2Hz, whereas only two pellets are required to achieve the target density of $4 \cdot 10^{19}$ $m^{-3}$ and a pellet frequency of ∼1 Hz is required to maintain it.

As for the power density on the divertor plates, even in the least favourable case (namely target density $4 \cdot 10^{19}$ $m^{-3}$ and background gas puff $1.0 \cdot 10^{21}$ $s^{-1}$) it did not exceed 2 MW $m^{-2}$ on the inner target and 3 MW $^{-2}$ on the outer target. It should be noted that the main effect on the core plasma of the reduction in background gas puff from $5.0 \cdot 10^{21}$ $s^{-1}$ to $1.0 \cdot 10^{21}$ $s^{-1}$ is a modest increase in the speed of the density decay after pellet injection, which could imply a slightly higher pellet frequency required to maintain the target volume-average density.

**Table 6.** Main plasma parameters achievable for different fuelling and heating conditions in an ITER D-T H-mode plasma at 10 MA / 5.3 T and 53 MW of additional power.

| Case | A | B | C |
|---|---|---|---|
| $P_{NBI}$ / $P_{ECRH}$ / $P_{ICRH}$ [MW] | 33 / - / 20 | 33 / - / 20 | 33 / - / 20 |
| $\Gamma_{D-T}$ [$10^{22}$ s$^{-1}$] / $\Gamma_{Ne}$ [$10^{20}$ s$^{-1}$] | 0.75 / - | 1.25 / - | 2.0 / - |
| $f_G$ | 0.5 | 0.6 | 0.7 |
| $n_e(0)$ / $< n_e >$ [$10^{19}$ m$^{-3}$] | 5.0 / 3.9 | 5.9 / 4.7 | 6.8 / 5.5 |
| $T_e(0)$ / $< T_e >$ [keV] | 17.1 / 8.9 | 15.7 / 7.7 | 14.4 / 6.8 |
| $T_i(0)$ / $< T_i >$ [keV] | 19.6 / 9.0 | 16.8 / 7.6 | 14.9 / 6.7 |
| $P_{fus}$ [MW] / $Q$ | 99.1 / 1.87 | 108.2 / 2.04 | 113.2/ 2.14 |
| Divertor material | Be | Be | Be |
| $Z_{eff}$ | 1.4 | 1.2 | 1.1 |
| $P_{IT}$ / $P_{OT}$ [MW m$^{-2}$] | 3.3 / 7.5 | 2.9 / 6.5 | 2.6 / 3.4 |

## 5. Results at 10 MA

For plasma current levels of 10 MA (and above) the picture of the density behaviour changes because the fusion power starts to play a role. The heat flux through the separatrix is increased by ∼20-25 MW due to alpha heating. This allows the achievement of a higher density at the separatrix by gas fuelling before the onset of detachment, which in turn allows for higher plasma densities in the core to be achievable by gas fuelling. The simulation results indicate that it may be difficult to maintain the ion temperature below the critical level for W sputtering on the outer target near the strike point location where the ion current density peaks in purely gas fuelled plasmas for $I_p \geq 10$ MA without Ne seeding. For this scenario, we carried out four series of runs. The first is a simple scan of the gas fuelling rate without pellet injection or Ne seeding, the second is a density scan obtained by varying the injection frequency of discrete pellets in presence of some Ne seeding, the third is a scan in the Ne seeding rate and the fourth is a study to analyze the sensitivity of the results to the width of the ETB.

### *5.1. Results 10 MA / 5.3 T / 53 MW.*

The results of the scan of the gas fuelling rate are summarized in table 6. It can be seen that for this particular heating and fuelling scheme $f_G \leq 0.7$ and $Q \approx 2$. Because of the relatively modest fusion power generated in this scenario, the power density on the divertor plate remains below 10 MW m$^{-2}$.

### *5.2. results at 10 MA / 5.3 T / 53 MW. Discrete pellets.*

The use of discrete pellets was analysed also in the case of a 10 MA, 5.3 T ITER D-T baseline H-mode case with 33 MW of NB and 20 MW of ICRH, continuous pellet, background D-T gas puff $1.0{\cdot}10^{22}$ s$^{-1}$ from the main chamber wall and $1.0{\cdot}10^{20}$ s$^{-1}$ Ne gas puff from the divertor region, which reached a steady-state volume-average density of $3.9{\cdot}10^{19}$ m$^{-3}$.

The reference simulation was continued for 1 s by replacing continuous with discrete pellets (mass $4.4{\cdot}10^{21}$ atoms, speed 300 m/s, composition 50-50 DT), requested by a feed-back mechanism that injected a pellet whenever the plasma volume-average density dropped below a prescribed level. The requested volume-average target densities were $4.5{\cdot}10^{19}$ $m^{-3}$and $6.7{\cdot}10^{19}$ $m^{-3}$. As for the simulations at 7.5 MA and 5.3 T, the higher level represents a Greenwald fraction equivalent to a volume-average density of $1.0{\cdot}10^{20}$ $m^{-3}$ at 15 MA, whereas the lower one is an intermediate value between the continuous pellet case and the highest density required. For each target volume-average density, we prescribed two levels of background gas puff, namely $7.5{\cdot}10^{21}$ $s^{-1}$ and $1.0{\cdot}10^{21}$ $s^{-1}$, to analyse the impact on the power load on the divertor. The results in figure 3 show that, in the case of target volume-average density $6.7{\cdot}10^{19}$ $m^{-3}$, seven pellets are requested at the maximum allowed frequency, but, shortly before reaching the target value, the particle throughput imposed on the plasma by such a high fuelling rate overloads the scrape-off layer with gas, forcing the detachment of the divertor and the numerical collapse of the simulation. The situation could be improved by increasing the duration of the minimum interval between consecutive pellets, by reducing the pellet mass or by reducing even more the back-ground gas-puff.

For the case with target volume-average density $4.5{\cdot}10^{19}$ $m^{-3}$, it can be seen that two pellets are needed to reach the reference value (figure 3, red curve). Once the requested volume-average density is reached a level of back-ground gas puff of $7.5{\cdot}10^{21}$ $s^{-1}$ is almost sufficient to fuel the plasma without the need of any further pellet injection, whereas with a lower back-ground gas puff of $1.0{\cdot}10^{21}$ $s^{-1}$ a pellet injection frequency of 1Hz would be required to maintain the volume-average plasma density at the prescribed value.

As for the divertor, we can see that at a gas puff rate of $7.5{\cdot}10^{21}$ $s^{-1}$ the power load remains below 3 MW $m^{-2}$ on the inner target and below 6 MW $m^{-2}$ on the outer target. Dropping the intensity of the gas puff to $1.0{\cdot}10^{21}$ increases the power density on the inner target to 7 MW $m^{-2}$ and on the outer target to just above 10 MW $m^{-2}$, indicating that such a low level of gas puff might not be enough for the safe operation of the ITER divertor.

### *5.3. Results at 10 MA / 5.3 T / 53 MW. Impurity seeding.*

In an attempt to see if it was possible further reduce the power loads to ≈5 MW $m^{-2}$ in a 10 MA, 5.3 T ITER D-T baseline H-mode plasma, we carried out simulations with additional Ne seeding on top of the D-T fuelling. The levels of D-T fuelling and Ne seeding used in the simulations are shown in table 7. The results (also shown in table 7) indicate that, even if the Ne seeding rate is increased up to $3.0{\cdot}10^{20}$ $s^{-1}$ (resulting in a in Ne content of to $1.3{\cdot}10^{21}$ particles and a rise in Ne radiation up to 18 MW), the effect on the electron target temperatures and the total power densities at the targets are minimal. Throughout the simulation the peak power densities at the inner and outer targets remain at ∼2.7 MW $m^{-2}$ and ∼8.0 MW $m^{-2}$ respectively. Only when we increase the D-T gas fuelling to $1.0{\cdot}10^{22}$ $s^{-1}$ the electron temperature at the targets clearly drops. Although these simulations did not meet the aim of reducing the target power loads to the projected 5 MW $m^{-2}$, the power load on the divertor target is acceptable from a machine safety point of view.

**Table 7.** Main plasma parameters achievable for different fuelling and heating conditions in an ITER D-T H-mode plasma at 10 MA / 5.3 T and 53 MW of additional power. (Ne seeding).

| Case | A | B | C |
|---|---|---|---|
| $P_{NBI}$ / $P_{ECRH}$ / $P_{ICRH}$ [MW] | 33 / - / 20 | 33 / - / 20 | 33 / - / 20 |
| $\Gamma_{D-T}$ [$10^{22}$ s$^{-1}$] / $\Gamma_{Ne}$ [$10^{20}$ s$^{-1}$] | 0.5 / 2.0 | 0.5 / 3.0 | 1.0 / 3.0 |
| $f_G$ | 0.47 | 0.46 | 0.46 |
| $n_e(0)$ / $< n_e >$ [$10^{19}$ m$^{-3}$] | 5.0 / 3.7 | 4.9 / 3.6 | 4.9 / 3.6 |
| $T_e(0)$ / $< T_e >$ [keV] | 17.5 / 9.5 | 17.8 / 9.6 | 17.8 / 9.6 |
| $T_i(0)$ / $< T_i >$ [keV] | 20.4 / 9.7 | 20.8 / 10.0 | 21.0 / 9.9 |
| $P_{fus}$ [MW] / $Q$ | 105.2 / 1.98 | 104.4 / 1.97 | 103.1 / 1.95 |
| Divertor material | Be | Be | Be |
| $Z_{eff}$ | 1.6 | 1.7 | 1.7 |
| $P_{IT}$ / $P_{OT}$ [MW m$^{-2}$] | 2.7 / 8.5 | 2.5 / 8.0 | 2.5 / 7.5 |

### *5.4. Results at 10 MA / 5.3 T / 53 MW. Sensitivity to ETB width.*

The JINTRAC simulations of D-T H-mode plasmas at 10 MA and 5.3 T show significant differences in terms of the predicted fusion performance. This is thought to be due to the strong non-linear dependence of the fusion power on the ion temperature at $T_i \approx 10$ keV in the plasma core, which is the typical value for the baseline scenario at 10 MA and 5.3 T. To show that this is indeed the case 1.5 dimensional core transport simulations were carried out with JETTO with varying ETB conditions and assumptions for the current density, particle pinch and the auxiliary heating scheme.

The boundary conditions at the separatrix for this series of simulations were taken from a full JINTRAC simulation of a purely gas fuelled D-T H-mode plasma at 10 MA and 5.3 T with $P_{aux} = 53$ MW (including 20 MW of ICRH) applying a constant D-T puff rate of $1.5{\cdot}10^{22}$ s$^{-1}$ and no Ne seeding. In terms of the normalized toroidal flux $\rho$, the width of the ETB was varied in the range 0.06-0.08 at constant $\alpha_c$, corresponding to a scan in pedestal pressure $p_{ped}$ in the range 50-70 kPa. The auxiliary heating was kept at a fixed total power of 53 MW but either 20 MW of ECRH or ICRH power were applied. Simulations were initialized with different current density profiles corresponding to internal inductance $l_i = 0.50$ and $l_i = 0.68$, respectively. A final simulation was carried out in which a collisionality dependence on the main ion pinch term was taken into account. The results are summarized in tables 8 and 9.

According to the results of the JETTO simulations, the fusion power obtained at 10 MA and 5.3 T can vary between 20-120 MW, corresponding to $Q$ in the range 0.3-2.3. Due to direct heating of core ions with ICRH giving higher core ion temperatures, the fusion power increases by ∼40 MW when ECRH is replaced by ICRH. The effect of the collisionality dependence of the particle pinch appears to be negligible, as the collisionality is already very low in 10 MA H-mode plasmas. For an increase of the width of 0.02 in terms of $\rho$ or, in other terms, for an increase in pedestal pressure of ∼20 kPa, the fusion power is almost doubled. It should be noted that, because of the dependence of the anomalous transport on the safety factor, the fusion performance is also significantly affected by the shape of the current density profile.

**Table 8.** Main plasma parameters achievable for different ETB and current profile assumptions in an ITER D-T H-mode plasma at 10 MA / 2.65 T and 53 MW of additional power. $\rho_{ETB}$ is the position of the top of the ETB in terms of normalized toroidal flux and $l_i$ is the plasma internal inductance.

| Case | A | B | C | D |
|---|---|---|---|---|
| $P_{NBI}$ / $P_{ECRH}$ / $P_{ICRH}$ [MW] | 33 / 20 / - | 33 / 20 / - | 33 / 20 / - | 33 / 20 / - |
| $\Gamma_{D-T}$ [$10^{22}$ s$^{-1}$] / $\Gamma_{Ne}$ [$10^{20}$ s$^{-1}$] | 1.5 / - | 1.5 / - | 1.5 / - | 1.5 / - |
| $f_G$ | 0.48 | 0.48 | 0.48 | 0.50 |
| $n_e(0)$ / $< n_e >$ [$10^{19}$ m$^{-3}$] | 4.8 / 3.8 | 4.9 / 3.8 | 4.9 / 3.8 | 4.8 / 3.9 |
| $T_e(0)$ / $< T_e >$ [keV] | 19.9 / 11.2 | 18.5 / 10.0 | 17.0 / 8.7 | 12.3 / 5.6 |
| $T_i(0)$ / $< T_i >$ [keV] | 15.9 / 9.4 | 14.4 / 8.3 | 13.0 / 7.2 | 8.4 / 4.4 |
| $P_{fus}$ [MW] / $Q$ | 103.5/ 1.95 | 80.6 / 1.52 | 60.2 / 1.14 | 21.3 / 0.40 |
| Divertor material | Be | Be | Be | Be |
| $Z_{eff}$ | 1.38 | 1.37 | 1.37 | 1.37 |
| $\rho_{ETB}$ | 0.92 | 0.93 | 0.94 | 0.94 |
| $l_i$ | 0.68 | 0.68 | 0.68 | 0.5 |

**Table 9.** Main plasma parameters achievable for different NBI, ECRH and ICRH combinations in an ITER D-T H-mode plasma at 10 MA / 2.65 T and 53 MW of additional power.

| Case | A | B |
|---|---|---|
| $P_{NBI}$ / $P_{ECRH}$ / $P_{ICRH}$ [MW] | 33 / 20 / - | 33 / - / 20 |
| $\Gamma_{D-T}$ [$10^{22}$ s$^{-1}$] / $\Gamma_{Ne}$ [$10^{20}$ s$^{-1}$] | 1.5 / - | 1.5 / - |
| $f_G$ | 0.48 | 0.48 |
| $n_e(0)$ / $< n_e >$ [$10^{19}$ m$^{-3}$] | 4.8/ 3.8 | 4.8 / 3.8 |
| $T_e(0)$ / $< T_e >$ [keV] | 18.5 / 10.0 | 18.2/ 9.7 |
| $T_i(0)$ / $< T_i >$ [keV] | 14.5 / 8.3 | 21.0 / 9.9 |
| $P_{fus}$ [MW] / $Q$ | 80.6/ 1.52 | 120.4 / 2.27 |
| Divertor material | Be | Be |
| $Z_{eff}$ | 1.37 | 1.37 |
| $\rho_{ETB}$ | 0.93 | 0.93 |
| $l_i$ | 0.68 | 0.68 |

## 6. Results at 15 MA

The bulk of the simulations performed for this study were done at 15 MA, 5.3 T and 53 MW of heating power. In this section we present a series of scans and sensitivity studies performed to analyse the fuelling of this scenario.

### *6.1. Results at 15 MA / 5.3 T / 53 MW. Be and W divertor.*

The first series of simulation was a series of JINTRAC runs performed for different gas rates both with Be and W divertor. The results are summarized in table 10 and 11, whereas in figure 1 we plot typical outer divertor power density profiles for the highest fuelling rates achievable with Be and W divertor respectively.

It can be seen that for these simulations relatively high gas puff rates ($3.0{\cdot}10^{22}$ s$^{-1}$ for Be divertor and $4.0{\cdot}10^{22}$ s$^{-1}$ for a W divertor) can be applied without lowering the temperature at the divertor targets to the point of detachment. This is due to the fact that the increased fusion power amplifies the heat flux crossing the separatrix, which maintains the divertor plasma away from detachment. The presence of an anomalous inward pinch in the core, due to the low plasma collisionality, also plays a role and leads to peaked core density profiles allowing to reach by gas fuelling only a volume average electron density of 6-7$\cdot10^{19}$ m$^{-3}$ in the Be divertor case and 6-10$\cdot10^{19}$ m$^{-3}$ in the W divertor case. In the simulations presented here the density at the separatrix was predicted to be in the range 5-6$\cdot10^{19}$ m$^{-3}$.

In the same simulations, the pressure at the top of the pedestal is ∼120-125 kPa, which is in good agreement with estimates from edge MHD stability modelling for ITER [8, 15]. Interestingly, for these gas fuelled plasmas the pressure increase in the pedestal zone is due almost exclusively to the large temperature gradient in the ETB, as the density profile in the ETB is almost flat. This is a consequence of the negligible neutral penetration across the separatrix into the core plasma and the lack of an anomalous pinch velocity in the ETB region assumed in this modelling. The results show that for a gas fuelling level of $3.0{\cdot}10^{22}$ s$^{-1}$, $Q \approx 7.5$ in the case of a Be divertor and $Q \approx 11.0$ in the case of a W divertor could be achieved, even if the effective core fuelling by neutrals remains at a level of $1.0{\cdot}10^{21}$ s$^{-1}$.

This high fusion performance without core fuelling by pellets is obtained in the simulations because it is assumed that the maximum achievable separatrix density by gas fuelling is only determined by the detachment limit in ITER H-modes and that increasing gas fuelling has no influence on the maximum pressure that can be achieved in the H-mode pedestal. Present experiments in H-mode plasmas show that increasing the plasma density by gas fuelling tends to decrease the pedestal pressure and the overall energy confinement in H-mode, which can be due to the increased plasma collisionality affecting the edge current magnitude and therefore the edge MHD stability or to the increased neutral penetration increasing transport in the ETB. It is presently unknown if such behaviour will be found in ITER or not, as some of the physics mechanisms invoked to explain present experimental results (i.e. decreased edge current density due to high collisionality or large core plasma neutral source) are not expected to play a significant role in ITER.

It is also important to note that these optimistic results for the core density and $Q$ achievable in ITER 15 MA plasmas with gas puffing rely on the presence of an anomalous pinch in the core, and, even more importantly, on assumptions of the reduction of anomalous transport in the SOL in H-mode plasmas. In these simulations it is assumed that the reduction of anomalous transport observed in the edge transport barrier slightly extends into the SOL. This is observed in present-day experiments and it is the physics mechanism invoked to explain the scaling of the scrape-off layer power deposition width in H-modes observed experimentally [16]. Without extension of at least a few millimetres of the low transport domain of the ETB beyond the separatrix, the heat flux would spread over a wider area on the target plates, due to the increased perpendicular transport, and detachment would be reached at much lower gas flux rates. This particular choice for the reduction of transport in the SOL of H-mode plasmas and the level of impurities at the divertor, which contribute to radiated power losses and to the decrease of the divertor temperature affecting the onset of the detachment, allows us to achieve a much higher level for the separatrix densities compared to original ITER studies [17]. These were performed with larger anomalous

**Table 10.** Main plasma parameters achievable for different fuelling and heating assumptions in an ITER D-T H-mode plasma at 15 MA / 5.3 T and 53 MW of additional power.

| Case | A | B | C |
|---|---|---|---|
| $P_{NBI}$ / $P_{ECRH}$ / $P_{ICRH}$ [MW] | 33 / - / 20 | 33 / - / 20 | 33 / - / 20 |
| $\Gamma_{D-T}$ [$10^{22}$ s$^{-1}$] / $\Gamma_{Ne}$ [$10^{20}$ s$^{-1}$] | 1.0 / - | 2.0 / - | 3.0 / - |
| $f_G$ | 0.48 | 0.52 | 0.58 |
| $n_e(0)$ / $< n_e >$ [$10^{19}$ m$^{-3}$] | 6.9 / 5.7 | 7.6 / 6.2 | 8.3 / 6.9 |
| $T_e(0)$ / $< T_e >$ [keV] | 20.7 / 12.0 | 20.1 / 11.4 | 19.4 / 10.7 |
| $T_i(0)$ / $< T_i >$ [keV] | 22.5 / 11.8 | 21.2 / 11.2 | 19.7 / 10.3 |
| $P_{fus}$ [MW] / $Q$ | 323.3 / 6.10 | 346.4 / 6.54 | 385.9 / 7.28 |
| Divertor material | Be | Be | Be |
| $Z_{eff}$ | 1.32 | 1.31 | 1.20 |
| $P_{IT}$ / $P_{OT}$ [MW m$^{-2}$] | 11.5 / 16.7 | 8.7 / 14.8 | 9.8 / 9.5 |

transport coefficients (uniform in the SOL) and C impurities. More recent studies carried out with transport coefficients similar to those in the integrated modelling presented here show similar values for the saturation of the separatrix density in ITER to those reported here [18].

The achievable separatrix density before the onset of detachment is also influenced by the presence of W (the dynamics of which is not considered in the study presented in this paper) and the puffing of Ne because of the associated increase of plasma radiative losses in the core and the SOL. It should be noted that large radiative losses are expected to be required in ITER for high Q D-T plasmas to maintain the peak divertor heat load below 10 MW m$^{-2}$. According to estimates of the power density impinging on the inner and outer target, reducing the peak divertor heat load under this limit requires gas fuelling levels higher than $2.0{\cdot}10^{22}$ s$^{-1}$ in addition to some level of Ne seeding compatible with a core Ne concentrations $\leq$0.5%.

It should be stressed that, before final conclusions for ITER can be drawn, a detailed quantitative validation of the integrated modelling approach applied to ITER with experimental results from gas fuelled H-mode density scans in present experiments is required. In the case of H-mode conditions this requires not only the validation of the SOL modelling assumptions setting the maximum achievable separatrix density but also of the MHD stability and transport assumptions in the ETB for H-mode plasmas with high plasma density, low pedestal collisionality and low neutral source in the pedestal region which require dedicated experiments at the highest currents and powers achievable in existing tokamaks to approach these ITER-like conditions.

### *6.2. Results at 15 MA / 5.3 T / 53 MW. Impurity seeding to reduce divertor power load below 10 MW m$^{-2}$.*

In the second scan performed for a 15 MA ITER H-mode D-T plasma, the JINTRAC simulations for purely gas fuelled H-mode plasmas at 15 MA, 5.3 T, 53 MW of auxiliary heating and a W divertor presented in section 6.1 were continued at fixed D-T gas puff rates of either $1.0{\cdot}10^{22}$ s$^{-1}$ or $3.0{\cdot}10^{22}$ s$^{-1}$ switching on Ne seeding at various levels in order to perform a scan in Ne gas puff rates. Ne seeding was applied from both

**Table 11.** Main plasma parameters achievable for different fuelling and heating assumptions in an ITER D-T H-mode plasma at 15 MA / 5.3 T and 53 MW of additional power.

| Case | A | B | C | D |
|---|---|---|---|---|
| $P_{NBI}$ / $P_{ECRH}$ / $P_{ICRH}$ [MW] | 33 / - / 20 | 33 / - / 20 | 33 / - / 20 | 33 / - / 20 |
| $\Gamma_{D-T}$ [$10^{22}$ s$^{-1}$] / $\Gamma_{Ne}$ [$10^{20}$ s$^{-1}$] | 1.0 / - | 2.0 / - | 3.0 / - | 4.0 / - |
| $f_G$ | 0.54 | 0.70 | 0.85 | 0.87 |
| $n_e(0)$ / $< n_e >$ [$10^{19}$ m$^{-3}$] | 7.9 / 6.4 | 10.1 / 8.3 | 12.3 / 10.1 | 12.6 / 10.4 |
| $T_e(0)$ / $< T_e >$ [keV] | 21.0 / 11.7 | 18.8 / 9.8 | 17.2 / 8.6 | 17.1 / 8.5 |
| $T_i(0)$ / $< T_i >$ [keV] | 21.0 / 11.1 | 17.9 / 9.3 | 16.1 / 8.2 | 15.9 / 8.1 |
| $P_{fus}$ [MW] / $Q$ | 443.3 / 8.36 | 520.0 / 9.81 | 591.5 / 11.16 | 608.2 / 11.48 |
| Divertor material | W | W | W | W |
| $Z_{eff}$ | 1.01 | 1.02 | 1.01 | 1.01 |
| $P_{IT}$ / $P_{OT}$ [MW m$^{-2}$] | 14.0 / 25.0 | 8.8 / 19.0 | 12.3 / 8.3 | 8.6 / 8.1 |

divertor target plates, while D-T gas was inserted from the top of the vessel. The results are summarized in table 12

According to the simulation results, Ne puff rates up to $\sim 1.5{\cdot}10^{19}$ s$^{-1}$ can be continuously applied in quasi-stationary purely gas fuelled H-mode plasmas at D-T gas puff rate of $\sim 1.0{\cdot}10^{22}$ s$^{-1}$. At higher Ne puff rates, the contamination of the core and SOL by Ne becomes too high and the plasma becomes thermally unstable. At $\Gamma_{Ne} = 1.25{\cdot}10^{19}$ s$^{-1}$, the Ne concentration in the core already amounts to $\sim$10% with $Z_{eff} \sim 1.9$ while the level of Ne radiation in the SOL reaches $\sim$30-35 MW. As expected, the plasma density is reduced with increased impurity contamination of the plasma. For the extreme case with $\Gamma_{Ne} = 1.25{\cdot}10^{19}$ s$^{-1}$, the volume averaged electron density drops from $6.8{\cdot}10^{19}$ m$^{-3}$ to less than $4.5{\cdot}10^{19}$ m$^{-3}$ and the fusion power is reduced from $\sim$450 MW to $\sim$300 MW due to plasma dilution.

It should be noted that Ne transport to the core is enhanced at lower D-T gas fuelling rates and therefore higher Ne core concentrations are reached when the Ne puff rates are adjusted to achieve a given level of Ne radiation in the SOL. In any case, simulation results tend to show that with a Ne puff rate of $\sim 1.0{\cdot}10^{19}$ s$^{-1}$ providing $\sim$30 MW of Ne radiation in the SOL, the maximum power density on the inner and outer targets could be reduced below the critical limit of 10 MW m$^{-2}$ and $Z_{eff} \approx 1.5$ could be maintained in the core. However, as a consequence of the low applied D-T gas puff rate, the ion temperature seems to remain above the critical limit of $\sim$5 eV for W sputtering in vicinity to the strike points where a peak in ion current density is expected.

It is interesting to note that the peak power density on the outer target does not monotonically decrease for increased Ne puff rates. For $\Gamma_{Ne} = 1.25{\cdot}10^{19}$ s$^{-1}$, the peak power density is larger than the one obtained with $\Gamma_{Ne} = 1.0{\cdot}10^{19}$ s$^{-1}$. This trend reversal seems to be related to transport assumptions for the ETB and the SOL. As the density is reduced at increased $\Gamma_{Ne}$, the pressure on top of the pedestal is maintained roughly constant by the continuous ELM model with fixed $\alpha_c$. Therefore, the temperature gradient increases, while the heat flux from the core tends to decrease because of the increased dilution and core radiated power. For this reason, the electron heat diffusivity must become lower for higher $\Gamma_{Ne}$. This eventually leads to a reduced

**Table 12.** Main plasma parameters achievable for different fuelling schemes in an ITER D-T H-mode plasma at 15 MA / 5.3 T and 53 MW of additional power. With Ne seeding.

| Case | A | B | C | D | E |
|---|---|---|---|---|---|
| $P_{NBI}$ / $P_{ECRH}$ / $P_{ICRH}$ [MW] | 33 / - / 20 | 33 / - / 20 | 33 / - / 20 | 33 / - / 20 | 33 / 0 / 20 |
| $\Gamma_{D-T}$ [$10^{22}$ s$^{-1}$] / $\Gamma_{Ne}$ [$10^{20}$ s$^{-1}$] | 1.0 / 0.010 | 1.0 / 0.075 | 1.0 / 0.100 | 1.0 / 0.125 | 3.0 / 0.010 |
| $f_G$ | 0.56 | 0.57 | 0.47 | 0.38 | 0.90 |
| $n_e(0)$ / $< n_e >$ [$10^{19}$ m$^{-3}$] | 8.4 / 6.7 | 8.4 / 6.8 | 7.1 / 5.6 | 5.7 / 4.5 | 13.0 / 10.7 |
| $T_e(0)$ / $< T_e >$ [keV] | 20.5 / 11.2 | 20.1 / 11.1 | 21.4 / 12.6 | 23.0 / 14.4 | 17.0 / 8.4 |
| $T_i(0)$ / $< T_i >$ [keV] | 20.3 / 10.6 | 20.1 / 10.6 | 22.9 / 12.4 | 27.3 / 15.0 | 15.8 / 8.0 |
| $P_{fus}$ [MW] / $Q$ | 456.5 / 8.61 | 448.2 / 8.46 | 385.0 / 7.27 | 312.5 / 5.90 | 624.5 / 11.78 |
| Divertor material | W | W | W | W | W |
| $Z_{eff}$ | 1.0 | 1.2 | 1.5 | 1.9 | 1.02 |
| $P_{IT}$ / $P_{OT}$ [MW m$^{-2}$] | 15.0 / 27.0 | 16.5 / 13.0 | 9.0 / 9.0 | 4.0 / 14.9 | 14.0 / 8.4 |

spread in heat deposition on the target causing larger power density peak values in vicinity to the strike points, although the total deposited power may actually be lower with increased Ne puff.

Comparing two cases with the same Ne puff rate $\Gamma_{Ne} = 1.0{\cdot}10^{18}$ s$^{-1}$ with low and high D-T gas puff rates of $\Gamma_{D-T} = 1.0{\cdot}10^{22}$ s$^{-1}$ and $\Gamma_{D-T} = 3.0{\cdot}10^{22}$ s$^{-1}$, the effect of enhanced Ne dissipation to the core for reduced $\Gamma_{D-T}$ can be illustrated. As shown in table 12, the plasma core and edge densities are enhanced and the plasma approaches detached conditions at $\Gamma_{D-T} = 3.0{\cdot}10^{22}$ s$^{-1}$, but the Ne content in the core remains lower ($\sim 1.4{\cdot}10^{19}$ Ne atoms) compared to the case with $\Gamma_{D-T} = 1.0{\cdot}10^{22}$ s$^{-1}$ ($\sim 2.0{\cdot}10^{19}$ Ne atoms). The Ne can be kept near the targets more efficiently with increased D-T gas fuelling due to an enhanced transfer of target-directed momentum from main ions to Ne particles via collisions in a high density environment.

### *6.3. Results at 15 MA / 5.3 T / 53 MW. Continuous pellet fuelling.*

As illustrated by the previous two series of simulations and the caveats about the fact that the result can be too optimistic, gas fuelling may be insufficient to achieve high fusion performance $Q \approx 10$ and the required core densities. However, pellet fuelling could allow to approach the Greenwald density limit while the density in the SOL can be maintained at a low level to avoid plasma detachment.

To investigate plasma operation in ELMy H-mode at high core density close to $Q \approx 10$, simulations were carried out for the flat-top phase of the ITER baseline scenario at 15 MA, 5.3 T and with W target using the continuous pellet fuelling model, continuing from a case in which the density in the core is already close to stationary conditions. 33 MW of NB heating and 20 MW of ECRH are applied to the plasma. D-T gas puff has either been completely switched off or set to fixed level of $1.0{\cdot}10^{22}$ s$^{-1}$. Pellets are assumed to be injected from the HFS of the vessel with a deposition profile centred at $\rho = 0.85$. A continuous pellet particle source profile with Gaussian shape and profile width of 0.2 in terms of $\rho$ is applied and rescaled to a given total particle source rate that is feedback controlled to maintain the line-averaged electron density close to a target value of $1.05{\cdot}10^{20}$ m$^{-3}$, which corresponds to 85-90% of the

Greenwald density limit.

The initial applied total pellet particle source rate amounts to $7.5{\cdot}10^{21}$ s$^{-1}$. The core transport for $\rho < 0.9$ has either been modelled with the Bohm/gyro-Bohm model plus the 'ad hoc' inward particle pinch described earlier in the paper or with GLF23. For $\rho > 0.9$ the Bohm/gyro-Bohm model has been applied in all cases. The model assumptions applied for the transport prediction in the ETB and SOL are the same as in the previous series of simulations. Be and Ne transport was taken into account. The applied Ne puff rate was varied during the simulations in order to achieve a scan between configurations with low Ne SOL radiation in the order of ∼5 MW and high Ne SOL radiation of up to ∼30-35 MW.

The main simulation results are summarized in table 13. The simulations indicate that a burning regime at high density approaching the ITER target of $Q \approx 10$ could be achieved with pellet fuelling. With the selected heating and fuelling configuration, the fusion power is predicted to vary around ∼480 MW, corresponding to $Q \approx 9.0$. The comparison of predictions with different core transport models demonstrates that GLF23 predictions are well approximated by the modified Bohm/gyro-Bohm model for high performance plasmas at $Q \leq 10$ in this ITER baseline scenario. In particular the prediction of the density peaking matches well, while typical differences can be observed in the details of the temperature profiles, with GLF23 predicting a steeper temperature gradient in the core and a shallower gradients further outside.

Without any D-T gas fuelling and low Ne radiation in the SOL of only a few MW, the peak power density on the outer target is estimated to be in a range of 30-40 MW m$^{-2}$. In addition, $T_i > 5$ eV everywhere on the targets except for the area interacting with the private region. Gas fuelling and Ne seeding seem to be mandatory to protect the target plates in the burning high $Q$ regime. According to simulation results, the power density can be reduced to a level close to or even below 10 MW m$^{-2}$ and the ion temperature be reduced below 5 eV in regions with maximum ion current density for a constant D-T gas puff rate of $1.0{\cdot}10^{22}$ s$^{-1}$ and Ne puff adjustment to reach a Ne SOL radiation level of 30-35 MW. To maintain the core density at a constant level of 85-90% of the Greenwald density limit in the quasi-stationary flat-top phase of the ITER 15 MA baseline scenario, a D-T pellet particle fuelling rate of $1.0\text{-}2.0{\cdot}10^{22}$ s$^{-1}$ is required.

### *6.4. Results at 15 MA / 5.3 T / 53 MW. Discrete pellet and impurity seeding.*

Although modelling pellet injection with the continuous pellet model can give some insight of what are the differences expected when the depth of the particle source is changed, it does not capture the intermittent nature of the pellet and the finite material retention time following the injection of a pellet. To model pellet fuelling in a more realistic way a discrete pellet model was used also for this scenario similarly to what was done for the 7.5 MA and 10 MA scenarios. The primary aim of this group of simulations task was to model the fuelling of a 15MA, 5.3T ITER D-T baseline H-mode with discrete pellets of various sizes to obtain $Q = 10$ and simultaneously find the maximum pellet size with acceptable divertor power load between pellets.

The cases analyzed and summarized in tables 14 and 15 were the continuation of a simulation with continuous pellets, background D-T gas puff $1.0{\cdot}10^{22}$ s$^{-1}$ from the main chamber wall and $1.0{\cdot}10^{20}$ s$^{-1}$ Ne seeding from the divertor region, which reached a volume-average density of $9.6{\cdot}10^{19}$ m$^{-3}$. The reference simulation was continued for 2.5 s by replacing continuous with discrete pellets of mass $4.4{\cdot}10^{21}$ atoms, speed

**Table 13.** Main plasma parameters achievable for different fuelling, heating and transport model assumptions in an ITER D-T H-mode plasma at 15 MA / 5.3 T and 53 MW of additional power. $\rho_p$ is the radial location of the barycentre (in terms of normalized toroidal flux), $\Delta_p$ is the full width at half maximum (FWHM) and $\Gamma_p$ is the time averaged intensity of the pellet particle source, which has a Gaussian radial profile.

| Case | A | B | C |
|---|---|---|---|
| $P_{NBI}$ / $P_{ECRH}$ / $P_{ICRH}$ [MW] | 33 / 20 / - | 33 / 20 / - | 32 / 20 / - |
| $\Gamma_{D-T}$ [$10^{22}$ s$^{-1}$] / $\Gamma_{Ne}$ [$10^{20}$ s$^{-1}$] | - / - | - / - | 1.0 / 1.0 |
| $\rho_p$ / $\Delta_p$ / $\Gamma_p$ [$10^{21}$ s$^{-1}$] | 0.85 / 0.2 / 12.0 | 0.85 / 0.2 / 12.1 | 0.85 / 0.2 / 9.2 |
| $f_G$ | 0.90 | 0.89 | 0.90 |
| $n_e(0)$ / $< n_e >$ [$10^{19}$ m$^{-3}$] | 13.3 / 10.7 | 13.2 / 10.6 | 13.5 / 10.7 |
| $T_e(0)$ / $< T_e >$ [keV] | 16.0 / 8.2 | 20.9 / 8.2 | 16.0 / 8.5 |
| $T_i(0)$ / $< T_i >$ [keV] | 14.0 / 7.7 | 17.7 / 7.7 | 14.0 / 7.8 |
| $P_{fus}$ [MW] / $Q$ | 460.7 / 8.69 | 478.9 / 9.04 | 499.8 / 9.43 |
| Divertor material | W | W | W |
| $Z_{eff}$ | 1.3 | 1.3 | 1.2 |
| $P_{IT}$ / $P_{OT}$ [MW m$^{-2}$] | 25.0 / 38.0 | 16.8 / 30.0 | 5.5 / 12.0 |
| Core transport model | Bohm/gyro-Bohm | GLF23 | Bohm/gyro-Bohm |

300m/s, composition 50-50 D-T and requiring the plasma volume-averaged density to be maintained at $1.0{\cdot}10^{20}$ m$^{-3}$. It can be seen from figure 4 that two pellets fired at the maximum allowed frequency of ∼6.5 Hz are needed to bring the volume-average density from the initial to the target value. Once the target value has been reached a pellet injection frequency of ∼2.1 Hz is needed to maintain the required volume-average density.

In order to explore the sensitivity of the simulation to the pellet mass and injection frequency, we performed two scans. In the first scan, starting from one second into the phase of the simulation where discrete pellets were used, we varied the pellet radius and injected pellets of mass $2.0{\cdot}10^{21}$, $2.7{\cdot}10^{21}$, $3.5{\cdot}10^{21}$, $4.4{\cdot}10^{21}$ and $5.5{\cdot}10^{21}$ atoms. For pellet masses above $5.5{\cdot}10^{21}$ atoms, the fuelling load imposed on the plasma was too high, the divertor reached a detached state shortly after the start of the run and the simulation could not be carried on until the end. However, delaying the injection of the first pellet by 0.5 s and allowing the density to decrease, made possible the injection of pellets of mass $6.1{\cdot}10^{21}$ atoms. This indicates that there is a maximum pellet mass allowed to avoid divertor detachment and that its value is sensitive to the pre-pellet density. In all the cases explored, we were able to maintain the required plasma volume-average density but the pellet frequency needed to do so change as illustrated in table 14.

In the second scan, we did not require any target volume-average density, but we fixed the pellet mass at $4.4{\cdot}10^{21}$ atoms and the pellet speed at 300 m/s and, starting from one second into the phase of the simulation fuelled by discrete pellets, we injected pellet at frequency of 3.5, 4.0, 4.5 and 5.0 Hz. The results for the range of frequencies explored are shown in table 15, where, for each pellet frequency, we report the corresponding rate of increase of the plasma volume-average density. It should be noted that the rate of change of the density cannot be maintained indefinitely, as for a given pellet frequency the plasma volume average density will saturate at a new

**Table 14.** Main plasma parameters achievable for different pellet sizes and frequencies in an ITER D-T H-mode plasma at 15 MA / 5.3 T and 53 MW of additional power. $m_p$ and $f_p$ are the pellet mass and frequency respectively.

| Case | A | B | C | D | E |
|---|---|---|---|---|---|
| $P_{NBI}$ / $P_{ECRH}$ / $P_{ICRH}$ [MW] | 33 / 20 / - | 33 / 20 / - | 33 / 20 / - | 33 / 20 / - | 33 / 20 / - |
| $\Gamma_{D-T}$ [$10^{22}$ s$^{-1}$] / $\Gamma_{Ne}$ [$10^{20}$ s$^{-1}$] | 1.0 / 0.01 | 1.0 / 0.01 | 1.0 / 0.01 | 1.0 / 0.01 | 1.0 / 0.01 |
| $m_p$ [$10^{21}$ atoms] / $f_p$ [Hz] | 2.0 / 3.6 | 2.7 / 2.5 | 3.5 / 2.3 | 4.4 /2.1 | 5.5 / 1.4 |
| $f_G$ | 0.85 | 0.85 | 0.88 | 0.85 | 0.88 |
| $n_e(0)$ / $< n_e >$ [$10^{19}$ m$^{-3}$] | 13.2 / 10.1 | 13.2 / 10.2 | 13.3 / 10.5 | 13.4 / 10.2 | 13.5 / 10.5 |
| $T_e(0)$ / $< T_e >$ [keV] | 16.4 / 8.7 | 16.3 / 8.7 | 16.3 / 8.5 | 16.2 / 8.7 | 16.2 / 8.5 |
| $T_i(0)$ / $< T_i >$ [keV] | 14.4 / 8.3 | 14.4 / 8.2 | 14.4 / 8.0 | 14.3 / 8.2 | 14.3 / 8.0 |
| $P_{fus}$ [MW] / $Q$ | 530.6 / 10.01 | 529.6 / 9.99 | 531.2 / 10.02 | 541.3 / 10.21 | 538.7 / 10.17 |
| Divertor material | W | W | W | W | |
| $Z_{eff}$ | 1.7 | 1.7 | 1.6 | 1.7 | 1.6 |
| $P_{IT}$ / $P_{OT}$ [MW m$^{-2}$] | 4.1 / 8.4 | 4.7 / 8.5 | 4.0 / 6.4 | 4.4 / 7.8 | 4.5 / 9.0 |

**Table 15.** Main plasma parameters achievable for different pellet frequencies in an ITER D-T H-mode plasma at 15 MA / 5.3 T and 53 MW of additional power. In this table $< \dot{n_e} >$ is the secular increase in volume average density resulting from pellet injection.

| Case | A | B | C | D |
|---|---|---|---|---|
| $P_{NBI}$ / $P_{ECRH}$ / $P_{ICRH}$ [MW] | 33 / 20 / - | 33 / 20 / - | 33 / 20 / - | 33 / 20 / - |
| $\Gamma_{D-T}$ [$10^{22}$ s$^{-1}$] / $\Gamma_{Ne}$ [$10^{20}$ s$^{-1}$] | 1.0 / 0.01 | 1.0 / 0.01 | 1.0 / 0.01 | 1.0 / 0.01 |
| $m_p$ [$10^{21}$ atoms] / $f_p$ [Hz] | 4.4 / 3.5 | 4.4 / 4.0 | 4.4 / 4.5 | 4.4 /5.0 |
| $< \dot{n_e} >$ [$10^{18}$ m$^{-3}$ s$^{-1}$] | 1.0 | 1.6 | 4.0 | 5.6 |
| $f_G$ | 0.85 | 0.85 | 0.88 | 0.94 |
| $n_e(0)$ / $< n_e >$ [$10^{19}$ m$^{-3}$] | 13.5 / 10.0 | 13.5 / 10.0 | 13.8 / 10.5 | 14.3 / 11.2 |
| $T_e(0)$ / $< T_e >$ [keV] | 16.8 / 10.1 | 16.9 / 9.2 | 16.9 / 9.5 | 16.7 / 9.0 |
| $T_i(0)$ / $< T_i >$ [keV] | 15.8 / 9.7 | 14.9 / 8.7 | 15.0 / 8.8 | 15.0 / 8.5 |
| $P_{fus}$ [MW] / $Q$ | 670.0 / 12.64 | 585.0 / 11.03 | 635.0 / 11.98 | 685.0 / 12.92 |
| Divertor material | W | W | W | W |
| $Z_{eff}$ | 1.7 | 1.6 | 1.6 | 1.6 |
| $P_{IT}$ / $P_{OT}$ [MW m$^{-2}$] | 6.2 / 10.4 | 4.2 / 7.5 | 4.3 / 6.0 | 4.1/ 6.4 |

equilibrium level. This can be seen in figure 5 for the 3.5 HZ pellets, where, after a barely visible increase caused by the first two pellets, the plasma volume-average density stops increasing and remains just below $1.0{\cdot}10^{20}$ m$^{-3}$.

As for the divertor power load, in the pellet mass scan it was similar in all the simulations performed and varied from 4.5 MW m$^{-2}$ on the inner target to 9.0 MW m$^{-2}$ on the outer target. The pellet frequency scan showed more variability and the power load on the divertor plates was 6.0 MW m$^{-2}$ on the inner target and 10 MW m$^{-2}$ on the outer target for the case with pellet frequency 3.5 Hz and 4.0 MW m$^{-2}$ on the inner target and 6.0 MW m$^{-2}$ on the outer target for the case with pellet frequency 5.0 Hz (the values for the intermediate cases were between these extremes).

*6.5. Results at 15 MA / 5.3 T / 53 MW. He accumulation.*

In purely gas-fuelled plasmas the removal of the He ashes from the core might be more challenging, as the core particle throughput is rather small because of the negligible particle source from the neutral beams and the neutrals penetrating from the edge and because of the particle transport to the SOL might be reduced in the inter-ELM phase due to the small density gradients in the ETB. It is therefore important to investigate whether problems related to He core accumulation like fuel dilution and energy radiation could become critical in gas fuelled, high $Q$, H-mode plasmas.

To this end, core transport simulations have been carried out with the JETTO/SANCO code with boundary conditions for the density, the temperature and the D-T neutral influx at the separatrix taken from a full JINTRAC simulation of a purely gas fuelled D-T H-mode plasma with W targets at a low fixed D-T puff rate of $\Gamma_{D-T} = 1.0 \cdot 10^{22}$ s$^{-1}$ presented previously. The core transport of the three impurities He, Be, and W is considered. The impurity densities are fixed at the separatrix to $n_{He} = 5 \cdot 10^{17}$ m$^{-3}$, $n_{Be} = 5 \cdot 10^{17}$ m$^{-3}$, $n_W = 5 \cdot 10^{15}$ m$^{-3}$. The impurity neutral influx at the separatrix is assumed to be negligible. Anomalous core transport is modelled by GLF23, considering impurity specific anomalous particle transport. The continuous sawtooth model is used to model the effect of sawteeth on heat and particle transport in the region affected by sawteeth. According to this model, $D$ and $\chi_{i,e}$ are increased (typically to values between 0.3 and 0.4 m$^2$ s$^{-1}$) inside the $q = 1$ surface to flatten the density and temperature profiles. Moreover, the value of the plasma resistivity at the $q = 1$ surface is extended inside this region to reduce the current density in the plasma core and, consequently, increase $q$ and the flux consumption. The core momentum transport with torque from neutral beams and $\chi_\phi = \chi_i$ is also taken into account. Because of the stabilising effect of rotational shear on microturbulence, the core confinement is improved and the fusion power increased ($P_{fus} \approx 450$ MW) compared to the full JINTRAC simulation (where $P_{fus} \approx 400$ MW). This configuration was selected for this study because this is where it is thought that the problems related to He core accumulation can become more apparent, due to the reduction in anomalous core transport and the increased production of He ash from the fusion reaction and operating at low density with a small gas flux rate of $\Gamma_{D-T} = 1.0 \cdot 10^{22}$ s$^{-1}$.

The results are summarized in table 16 (case A), from which it can be seen that, in the best performing case, $Q \approx 9$. In these conditions, the He ash production rate amounts to $\sim 1.6 \cdot 10^{20}$ s$^{-1}$. Inspecting the density and effective diffusivity profiles for the main ions (shown in figure 6), it can be seen that GLF23 predicts an anomalous inwards pinch for the main ions. This can be concluded from the fact that the effective diffusivity for D and T is close to zero (and, at times, even negative) across a wide region of the plasma, causing non-zero density gradients for both D and T even in absence of T core sources. On the other side, the anomalous He transport is almost purely diffusive as it can be seen form figure 7), which shows the He density and the He total diffusivity and convective velocity (neoclassical plus anomalous). Some small fluctuations in He pinch velocity are present in the edge region and can be attributed to neoclassical transport. Although a strong outward neoclassical pinch is predicted for the ETB region for high $Z$ impurities, leading to almost complete screening of W from the core and very steep W density gradients in vicinity to the separatrix, the temperature screening is still present for He but it is too small ($v_{He} < 0.1$ m s$^{-1}$) to have a noticeable effect on the He transport in the core.

**Table 16.** Main plasma parameters achievable in an ITER D-T H-mode plasma at 15 MA / 5.3 T and 53 MW of additional power taking into account He, Be and W as impurities. Case A: $n_{He}(\rho = 1) = 5{\cdot}10^{17}$ m$^{-3}$; case B: $n_{He}(\rho = 1) = 6{\cdot}10^{18}$ m$^{-3}$.

| Case | A | B |
|---|---|---|
| $P_{NBI}$ / $P_{ECRH}$ / $P_{ICRH}$ [MW] | 33 / 20 / - | 33 / 20 / - |
| $\Gamma_{D-T}$ [$10^{22}$ s$^{-1}$] / $\Gamma_{Ne}$ [$10^{20}$ s$^{-1}$] | 1.0 / - | 1.0 / - |
| $f_G$ | 0.57 | 0.66 |
| $n_e(0)$ / $< n_e >$ [$10^{19}$ m$^{-3}$] | 8.9 / 6.8 | 9.9 / 7.9 |
| $T_e(0)$ / $< T_e >$ [keV] | 28.4 / 11.9 | 26.1 / 10.6 |
| $T_i(0)$ / $< T_i >$ [keV] | 20.9 / 10.7 | 20.0 / 10.0 |
| $P_{fus}$ [MW] / $Q$ | 447.9 / 8.45 | 401.6 / 7.58 |
| Divertor material | W | W |
| $Z_{eff}$ | 1.08 | 1.19 |

As a result, the core He density (shown in figure 7) is slightly peaked due to the He source originating from the fusion reactions taking place in the core. Moreover, although the main ion density profile is flat in the ETB region, an edge pedestal develops in the He density, which can also be explained by the location of the He source in the core. The average anomalous diffusivity is significantly larger for He (up to $D_{He} \approx 5$ m$^2$ s$^{-1}$) compared to the main ions ($D_{D,T} \leq 0.2$ m$^2$ s$^{-1}$) and it decreases towards the core in line with $\chi_{i,e}$. For this reason, the peaking in He density is very small ($n_{He}(\rho = 0)/n_{He}(\rho = 1) \approx 1.3$) and essentially caused by increased He density gradients in the region close to the magnetic axis where the anomalous He transport is almost fully suppressed and He is transported due to sawteeth and neoclassical diffusion only. The He core concentration amounts to ∼1.5%, therefore the core dilution due to the He is negligible in this case. However, the He core concentration strongly depends on the He density and the He neutral influx at the separatrix, which has been prescribed and may have been underestimated.

According to equation (6) and (7) in [17], $n_{He}$ in the range 2-6·$10^{18}$ m$^{-3}$ and $\Gamma_{He} \leq 2 \cdot 10^{20}$ s$^{-1}$ can be expected due to a rather low normalized pressure $\gamma$ in the range 0.2-0.4 related to the low level of gas fuelling in this configuration. To test the effect of these parameters on the results, a second simulation was performed imposing $n_{He} = 6 \cdot 10^{18}$ m$^{-3}$ and $\Gamma_{He} = 2 \cdot 10^{20}$ s$^{-1}$ at the separatrix. The results are also reported in table 16 (case B). One can see that the He concentration is increased to ∼5-7%. However, the effect on the dilution is marginal even in this case: compared to the simulation at $n_{He} = 5 \cdot 10^{17}$ m$^{-3}$, $P_{fus}$ is reduced from ∼450 MW to ∼400 MW. Due to profile stiffness, the He density profile is increased everywhere by 5.5·$10^{18}$ m$^{-3}$ and the peaking is reduced to $n_{He}(\rho = 0)/n_{He}(\rho = 1) \approx 1.07$.

The anomalous He core transport is further enhanced reaching maximum diffusivities of $D_{He} \approx 8$ m$^2$s$^{-1}$. This strong predicted level of He transport is the main reason why, even in this extreme conditions of low D-T throughput, fuelling by gas only and taking into account the stabilizing affect of the rotational shear, He ash contamination of the core plasma remains tolerable and the modelling results suggest that it may be possible to keep He accumulation in the core at an acceptable level in ITER baseline scenario configurations with gas fuelling only also at low D-T gas rates.

### *6.6. Results 15 MA / 5.3 T / 53 MW. He accumulation with pellet fuelling.*

The JINTRAC simulations for gas and pellet fuelled high $Q$ H-mode plasmas at 15 MA, 5.3 T and 53 MW of auxiliary heating power (33 MW NBI and 20 MW ECRH) with W target presented previously have been repeated at a fixed D-T gas puff rate of $1.0 \cdot 10^{22}$ s$^{-1}$ with Ne seeding. The He and Ne transport was taken into account and the Ne seeding was adjusted in order to provide a Ne radiation level in the SOL of ∼30 MW. Pellets are modelled with the HPI2 code with pellet size $m_p = 5.5 \cdot 10^{21}$ atoms, velocity $v_p = 300$ m/s, 50-50 D-T mixture and injection from the upper HFS. The pellet injection frequency is adjusted in order to maintain a line-averaged electron density of $1.0{\cdot}10^{20}$ m$^{-3}$. The He is produced due to the fusion reactions in the core. The simulation is continued for several tens of seconds until stationary conditions are approached for the He density in the core and edge regions.

The main simulation results are summarized in table 17. According to simulation results, the maximum power density on the inner and outer targets can be maintained below 10 MW m$^{-2}$ with the applied D-T and Ne puff rates. To achieve a Ne radiation level in the SOL of ∼30 MW, an average Ne seeding rate of $\sim 1.0{\cdot}10^{19}$ s$^{-1}$ is necessary. The ion temperature can be kept below the critical level for W sputtering of ∼5 eV in a region approximately 5 cm wide near the strike-point location on the outer target where the absolute ion current density peak is located. To maintain the density at a level of ∼85% of the Greenwald density limit, pellets with the standard ITER size need to be injected at a time-averaged frequency of ∼2-2.5 Hz which is in line with previous core transport fuelling studies as presented in [19].

The He density at the separatrix saturates at $\sim 2.5{\cdot}10^{18}$ m$^{-3}$, while the He density on axis approaches $\sim 6{\cdot}10^{18}$ m$^{-3}$, corresponding to a core He peaking factor of ∼2.4. This peaking factor is considerably larger than the one obtained in core-only simulations with GLF23 with comparable on-axis He density. This is due to differences in predictions for the He core diffusivity, which is assumed to be identical to the diffusivity for main ions with the modified Bohm/gyro-Bohm transport model and thus much lower than the $D_{He}$ predicted with GLF23.

In quasi-stationary conditions the time-averaged He pump rate is identical to the He source rate due to fusion reactions in the core, which is $\sim 1.75{\cdot}10^{20}$ s$^{-1}$. As a consequence of increased plasma dilution, a slight degradation in fusion performance with respect to similar simulations without He from $P_{fus} \approx 550$ MW to $P_{fus} \approx 490$ MW is predicted, as the He concentration increases from ∼2% to ∼4.5%. $Z_{eff} \approx 1.35$ in stationary conditions. Due to temperature screening in the edge region, the core Ne density can be kept at a comparably low level in the range $2.5\text{-}3.0{\cdot}10^{17}$ m$^{-3}$, corresponding to a Ne core concentration of ∼0.25%. Without the temperature screening effect, the core Ne density could increase by $\sim 1.0{\cdot}10^{17}$ m$^{-3}$ for the same Ne density at the separatrix. The total core radiation in stationary conditions amounts to ∼25 MW. Very similar results are obtained in another set of runs at a slightly reduced target Ne radiation in the SOL of ∼28 MW.

### *6.7. Results at 15 MA / 5.3 T / 53 MW. Sensitivity to bootstrap current density in pellet and gas fuelled plasmas.*

Differences in edge density and bootstrap current have been studied for full JINTRAC simulations of purely gas fuelled and pellet fuelled plasmas at 15 MA, 5.3 T and 53 MW of auxiliary power with W targets. A comparison of plasma profiles is shown

**Table 17.** Main plasma parameters achievable in an ITER D-T H-mode plasma at 15 MA / 5.3 T and 53 MW of additional power taking into account He, Be and W as impurities. Ne seeding adjusted to obtain a fixed level of radiated power in the SOL (case A: 30 MW; case B: 28 MW).

| Case | A | B |
|---|---|---|
| $P_{NBI}$ / $P_{ECRH}$ / $P_{ICRH}$ [MW] | 33 / 20 / - | 33 / 20 / - |
| $\Gamma_{D-T}$ [$10^{22}$ s$^{-1}$] / $\Gamma_{Ne}$ [$10^{20}$ s$^{-1}$] | 1.0 / 0.1 | 1.0 / 0.1 |
| $m_p$ [$10^{21}$ atoms] / $f_p$ [Hz] | 5.5 / 2.3 | 5.5 / 2.4 |
| $f_G$ | 0.82 | 0.83 |
| $n_e(0)$ / $< n_e >$ [$10^{19}$ m$^{-3}$] | 12.5 / 9.7 | 12.6 / 9.9 |
| $T_e(0)$ / $< T_e >$ [keV] | 16.7 / 9.4 | 16.6 / 9.2 |
| $T_i(0)$ / $< T_i >$ [keV] | 14.9 / 8.8 | 14.9 / 8.7 |
| $P_{fus}$ [MW] / $Q$ | 497.3 / 9.38 | 482.4 / 9.10 |
| Divertor material | W | W |
| $Z_{eff}$ | 1.35 | 1.42 |
| $P_{IT}$ / $P_{OT}$ [MW m$^{-2}$] | 6.6 / 5.8 | 5.5 / 5.6 |

**Table 18.** Main plasma parameters achievable under different edge plasma kinetic profiles and bootstrap current in an ITER D-T H-mode plasma at 15 MA / 5.3 T and 53 MW of additional power.

| Case | A | B | C |
|---|---|---|---|
| $P_{NBI}$ / $P_{ECRH}$ / $P_{ICRH}$ [MW] | 33 / 20 / - | 33 / - / 20 | 33 / - / 20 |
| $\Gamma_{D-T}$ [$10^{22}$ s$^{-1}$] / $\Gamma_{Ne}$ [$10^{20}$ s$^{-1}$] | - / - | - / - | 4.0 / - |
| $\rho_p$ / $\Delta_p$ / $\Gamma_p$ [$10^{21}$ s$^{-1}$] | 0.85 / 0.2 / 12.0 | - | - |
| $f_G$ | 0.90 | 0.75 | 0.87 |
| $n_e(0)$ / $< n_e >$ [$10^{19}$ m$^{-3}$] | 13.3 / 10.7 | 13.6 / 8.9 | 12.6 / 10.4 |
| $T_e(0)$ / $< T_e >$ [keV] | 16.0 / 8.2 | 17.2 / 10.2 | 17.1 / 8.5 |
| $T_i(0)$ / $< T_i >$ [keV] | 14.0 / 7.7 | 17.0 / 9.9 | 15.9 / 8.1 |
| $P_{fus}$ [MW] / $Q$ | 460.7 / 8.7 | 585.9 / 11.1 | 608.2 / 11.5 |
| Divertor material | W | W | W |
| $Z_{eff}$ | 1.26 | 1.48 | 1.01 |
| $P_{IT}$ / $P_{OT}$ [MW m$^{-2}$] | 24.6 / 37.8 | 11.7 / 23.0 | 8.6 / 8.1 |

in figures 9 and 10 for three cases with continuous pellet fuelling, with pellet fuelling having been switched off before the start of the simulation and a gas fuelling rate $\Gamma_{D-T} = 4.0 \cdot 10^{22}$ s$^{-1}$. The results of the simulations are summarized in table 18.

Although densities and temperatures are well comparable for the three cases in the core region, the edge densities deviate strongly. In the purely gas fuelled case, the density profile is almost flat in the ETB region which is due to negligible particle sources from the core, negligible particle pinch in the ETB and a very low flux of neutrals crossing the separatrix. For the pellet fuelled case however, a significant density gradient is predicted to appear in the ETB as a consequence of low particle diffusivities in the ETB and significant core particle sources due to pellet fuelling. Due to these differences in density gradient, one would expect deviations in bootstrap

current densities that could affect pedestal stability, as the influence of the density gradient on the bootstrap current density dominates that of the electron and ion temperatures for similar values of logarithmic density and temperature gradients. However, for the three cases analysed, the variation in bootstrap current is rather small.

The bootstrap current density, $j_{bs}$, has been predicted by the NCLASS model. Despite small deviations in the order of ∼20% in edge bootstrap current density, the predictions for $j_{bs}$ do not appear to be in contradiction with the expression for $j_{bs}$ given in [20]. Although $dn_i/d\rho$ is reduced to zero in the case with strong gas fuelling and the collisionality is considerably increased due to higher densities in the ETB causing a reduction in bootstrap current, only a slight decrease in bootstrap current density can be expected compared to the case with pellet fuelling, as the terms proportional to the temperature gradients are dominant in these situations. As shown in figure 10, the logarithmic derivative of the electron temperature is up to two orders of magnitude larger than that of the electron density. It should be noted that the density at the separatrix is rather high for the case with pellet fuelling ($\sim 6 \cdot 10^{19}$ m$^{-3}$) compared to typical configurations with pellet fuelling, which is related to a rather low impurity contamination in the edge ($Z_{eff} < 1.1$).

For higher impurity concentrations and lower density at the separatrix, the density gradient in the ETB is expected to increase by a factor ∼2.0. The difference in bootstrap current density for purely gas fuelled and pellet fuelled configurations might then become more important, although the temperature gradient driven bootstrap current is likely to remain dominant. It is worth noting that a possible change in edge MHD stability due to a reduction in edge bootstrap current for purely gas fuelled plasmas has not been considered in the simulations presented in this study, where $\alpha_c$ was assumed to be the same for pellet fuelled and gas fuelled plasmas. The MHD stability may need to be reassessed for purely gas fuelled plasma configurations, although it is not expected to deviate strongly from the case of pellet fuelled plasmas as has been demonstrated in this analysis, since pressure gradients and current densities are not substantially different.

### *6.8. Results 15 MA / 5.3 T / 53 MW sensitivity to MHD peeling-ballooning stability limit ($\alpha_c$).*

To investigate the sensitivity of the simulation results obtained with full JINTRAC to the assumptions for the pedestal width and ETB transport, scans have been carried out for purely gas fuelled D-T H-mode plasmas at 15 MA, 5.3 T, and 53 MW of auxiliary heating power with W target for high and medium gas puff rates of $\Gamma_{D-T} = 1.0 \cdot 10^{22}$ s$^{-1}$ and $\Gamma_{D-T} = 2.5 \cdot 10^{22}$ s$^{-1}$.

In this series of simulations, instead of prescribing the ETB according to the EPED1 model predictions (as it was done in most of the simulations presented in this paper), we varied it in order to scan the location of the top of the pedestal in the range between $\rho = 0.91$ and $\rho = 0.95$, while the maximum allowed normalized pressure gradient in the ETB (which is controlled by the continuous ELM model) was increased from $\alpha_c = 1.38$ to $\alpha_c = 3.20$ in order to maintain the pressure at the the top of the ETB around ∼130 kPa. In this way, the uncertainty in predictions for plasma confinement and fusion performance due to uncertainties in the pedestal width for a given pedestal pressure can be estimated. The results for the two levels of gas rate are summarized in table 19 and 20.

For the range of $\alpha_c$ and ETB width at constant pedestal pressure investigated, a variation in fusion power of ∼200 MW was found for both scans at low and medium gas puff rates. For the scan at $\Gamma_{D-T} = 1.0 \cdot 10^{22}$ s$^{-1}$, $Q$ varies between 8.5 and 12.5 while, at $\Gamma_{D-T} = 2.5 \cdot 10^{22}$ s$^{-1}$, $Q$ varies between 10.0 and 14.0. It should be noted that the impurity concentration in these plasmas is very low with $Z_{eff} \sim 1.01$. This is a consequence of considering W targets without taking into account at the same time W impurity transport, not taking into account the presence of He, a negligible Be sputtering at the walls and no Ne seeding, all of which imply that, in the modelling, very high densities can be achieved with gas fuelling only.

Differences in fusion performance can be attributed to differences in predictions for the separatrix density that determines the level of core density and influences the fusion reaction rate in the core, which scales as $n_D n_T$. For both scans at low and medium gas puff rates, the D density at the separatrix is in the range 2.0-2.2·10$^{19}$ m$^{-3}$. This variation is related to a change in transport coefficients in the near SOL, as the latter are determined by the transport coefficients applied in the ETB. The higher $\alpha_c$ in the ETB, the lower become the continuous ELM model predictions for $D$, $\chi_e$ and $\chi_i$, as lower transport coefficients are required to maintain a higher pedestal pressure in the ETB. As diffusion in the near SOL is reduced with lower $D$, $\chi_e$ and $\chi_i$, the density and temperature gradients in that region are increased and higher separatrix densities are achieved for higher $\alpha_c$.

It should be pointed out that the predicted variation in the density at the separatrix and the associated change in fusion performance seems to be almost entirely due to the assumption that the ETB transport is extended by a few millimetres into the SOL. Without this assumption, the transport in the near SOL would not be affected by a variation in $\alpha_c$ or in the ETB width, the density in the near SOL would remain similar, and thus similar separatrix density and fusion power predictions would be obtained. A sensitivity scan with respect to the ETB extension into the SOL will be presented in the next subsection.

It is also worth noting that the simulation assumptions for the scans in $\alpha_c$ are questionable not only with respect to impurity contamination but also in view of divertor conditions. The limit of 10 MW m$^{-2}$ is exceeded for all cases at low and medium gas puff rate at least on one target plate, as the total heat flux from the core is very large and no Ne seeding has been applied. However, the ion temperature near the strike point locations can be maintained below the critical level for W sputtering of 5 eV at least for the cases at $\Gamma_{D-T} = 2.5 \cdot 10^{22}$ s$^{-1}$.

### *6.9. Results at 15 MA / 5.3 T / 53 MW. Sensitivity to ETB extension in the SOL.*

As mentioned above, the assumption of an extension of the ETB into the SOL can be expected to have a strong influence on predicted plasma conditions. To test the sensitivity of the results to this assumption, we carried out a scan of the width of the ETB extension into the SOL, based on the full JINTRAC simulations of purely gas fuelled D-T H-mode plasmas at 15 MA, 5.3 T, 53 MW of auxiliary heating power and with W targets. The results are summarized in table 21, where simulation results are shown for a case with an ETB extension into the SOL of ∼6 mm on the outer mid-plane (which is the standard assumption for all H-mode plasma simulations presented in this paper) at a low D-T gas puff rate of $\Gamma_{D-T} = 1.0 \cdot 10^{22}$ s$^{-1}$, and for cases without an ETB extension into the SOL at fixed D-T gas puff rates of $\Gamma_{D-T} = 1.0 \cdot 10^{22}$ s$^{-1}$, $\Gamma_{D-T} = 2.0 \cdot 10^{22}$ s$^{-1}$ and $\Gamma_{D-T} = 3.0 \cdot 10^{22}$ s$^{-1}$. No Ne seeding was used in these

**Table 19.** Main plasma parameters achievable for different ETB width and normalized critical pressure gradient $\alpha_c$ assumptions in an ITER D-T H-mode plasma at 15 MA / 5.3 T and 53 MW of additional power. (Low gas rate).

| Case | A | B | C |
|---|---|---|---|
| $P_{NBI}$ / $P_{ECRH}$ / $P_{ICRH}$ [MW] | 33 / - / 20 | 33 / - / 20 | 33 / - / 20 |
| $\Gamma_{D-T}$ [$10^{22}$ s$^{-1}$] / $\Gamma_{Ne}$ [$10^{20}$ s$^{-1}$] | 1.0 / - | 1.0 / - | 1.0 / - |
| $f_G$ | 0.56 | 0.71 | 0.82 |
| $n_e(0)$ / $< n_e >$ [$10^{19}$ m$^{-3}$] | 8.3 / 6.7 | 10.3 / 8.4 | 11.8 / 9.7 |
| $T_e(0)$ / $< T_e >$ [keV] | 20.0 / 10.7 | 18.7 / 9.8 | 18.2 / 9.4 |
| $T_i(0)$ / $< T_i >$ [keV] | 19.9 / 10.2 | 17.8 / 9.3 | 17.1 / 8.9 |
| $P_{fus}$ [MW] / $Q$ | 426.2 / 8.04 | 534.2 / 10.08 | 630.5 / 11.90 |
| Divertor material | W | W | W |
| $Z_{eff}$ | 1.01 | 1.01 | 1.01 |
| $P_{IT}$ / $P_{OT}$ [MW m$^{-2}$] | 20.0 / 15.5 | 29 / 16.0 | 38.5 / 18.3 |
| $\rho_{ETB}$ / $\alpha_c$ | 0.91 / 1.38 | 0.93 / 1.9 | 0.85 / 3.2 |

**Table 20.** Main plasma parameters achievable for different ETB width and normalized critical pressure gradient $\alpha_c$ assumptions in an ITER D-T H-mode plasma at 15 MA / 5.3 T and 53 MW of additional power. (Medium gas rate).

| Case | A | B | C |
|---|---|---|---|
| $P_{NBI}$ / $P_{ECRH}$ / $P_{ICRH}$ [MW] | 33 / - / 20 | 33 / - / 20 | 33 / - / 20 |
| $\Gamma_{D-T}$ [$10^{22}$ s$^{-1}$] / $\Gamma_{Ne}$ [$10^{20}$ s$^{-1}$] | 2.5 / - | 2.5 / - | 2.5 / - |
| $f_G$ | 0.82 | 0.90 | 1.00 |
| $n_e(0)$ / $< n_e >$ [$10^{19}$ m$^{-3}$] | 11.8 / 9.7 | 13.0 / 10.7 | 14.5 / 11.9 |
| $T_e(0)$ / $< T_e >$ [keV] | 17.0 / 8.4 | 17.1 / 8.4 | 17.0 / 8.4 |
| $T_i(0)$ / $< T_i >$ [keV] | 16.0 / 8.0 | 15.8 / 8.0 | 15.7 / 8.0 |
| $P_{fus}$ [MW] / $Q$ | 538.1 / 10.15 | 626.4 / 11.82 | 762.6 / 14.39 |
| Divertor material | W | W | W |
| $Z_{eff}$ | 1.00 | 1.00 | 1.01 |
| $P_{IT}$ / $P_{OT}$ [MW m$^{-2}$] | 14.0 / 8.7 | 16.0 / 9.0 | 24.0 / 12.5 |
| $\rho_{ETB}$ / $\alpha_c$ | 0.91 / 1.38 | 0.93 / 1.9 | 0.85 / 3.2 |

simulations. As a consequence, the impurity concentration was very low, resulting in $Z_{eff} \leq 1.01$.

As expected, the predicted plasma performance is significantly affected by the assumption of an ETB extension of a few millimetres into the SOL. For two cases at low gas puff rate with and without ETB extension, the predicted fusion power varies by ∼80 MW. Without ETB extension, $Q \approx 7.7$, while with an ETB extension of ∼6 mm $Q \approx 9.2$ is obtained. Similarly to the scan in ETB width presented in the previous subsection, the change in plasma performance is directly linked to a change in density at the separatrix, which largely determines the density in the core and thus the fusion reaction rate. Without a reduction of the transport extended from the ETB into the near SOL, the transport coefficients prescribed for the far SOL are applied everywhere in the SOL up to the separatrix. These transport coefficients

are much larger than those predicted for the ETB region with the continuous ELM model. For this reason, the temperature and density gradients in the near SOL are reduced without ETB extension compared to the case with an ETB extension. As for the density, this effect is comparably small. The jump in density over the first ∼5 mm in the near SOL on the outer mid-plane is only changed from ∼$0.75{\cdot}10^{19}$ $m^{-3}$ to ∼$1.5{\cdot}10^{19}$ $m^{-3}$ with application of an ETB extension. On the other hand the jump in temperature increases from ∼50 eV to ∼300 eV. Consequently, with much higher temperatures near the separatrix on the outer mid-plane, the plasma energy is also considerably enhanced near the strike-point positions on the target plates, where the recycling process is localized. Due to the higher plasma energy in this region, recycled neutrals are more likely to be ionized again, and a lower amount of recycled neutrals can escape the SOL. For this reason the overall plasma density in the SOL is increased compared to the case without ETB extension in stationary conditions for the same gas puff rates and approximately identical pump rates. As the parallel heat flux decay length $\lambda_q$ is reduced for reduced transport coefficients in the near SOL with an ETB extension into the SOL, the power is deposited on the target plates in a narrower region near the strike-point location. For this reason, the maximum power density on the target plates is considerably larger if an ETB extension is taken into account.

Applying a scan in gas puff rates with zero ETB extension into the SOL, similar variations in fusion power and density are achieved as for a scan in $\Gamma_{D-T}$ with non-zero ETB extension, however, detachment may be achieved already at lower $\Gamma_{D-T}$. As can be seen from table 21, the increase in density for cases with $\Gamma_{D-T} = 3.0 \cdot 10^{22}$ $s^{-1}$ with respect to cases with $\Gamma_{D-T} = 2.0 \cdot 10^{22}$ $s^{-1}$ is reduced compared with the increase between cases with $\Gamma_{D-T} = 2.0 \cdot 10^{22}$ $s^{-1}$ and $\Gamma_{D-T} = 1.0 \cdot 10^{22}$ $s^{-1}$. This is an indication that detached conditions are already approached at $\Gamma_{D-T} = 3.0 \cdot 10^{22}$ $s^{-1}$. A similar reduction of the density increment was observed for the same scan with non-zero ETB extension around $\Gamma_{D-T} = 4.0 \cdot 10^{22}$ $s^{-1}$, as shown previously. Due to lower predicted separatrix densities with zero ETB extension for the same D-T gas puff rate, $Q$ is reduced compared to similar plasma configurations with non-zero ETB extension. At the maximum applicable gas puff rates with zero ETB extension we obtain $Q \leq 10$ even for a pure plasma with $Z_{eff} \approx 1.0$. At higher gas puff rates, it seems to be possible to keep the maximum power density below 10 MW $m^{-2}$ and to maintain $T_i < 5$ eV near the strike-point locations on both targets with zero ETB extension into the SOL even for pure plasmas without Ne seeding (but neglecting W sputtering and transport) due to increased $\lambda_q$.

### *6.10. Results at 15 MA / 5.3 T / 53 MW. Gas fuelling rate scan with fixed transport in the SOL.*

JINTRAC simulations of purely gas fuelled D-T H-mode plasmas at 15 MA, 5.3 T, auxiliary heating power 53 MW and with W targets have been repeated with the same assumptions for SOL transport as used in previous edge modelling studies for ITER as, for example, in [18]. In particular, fixed constant transport coefficients $D = 0.3$ $m^2s^{-1}$, $\chi_e = \chi_i = 1.0$ $m^2s^{-1}$ have been applied everywhere in the SOL. The D-T gas puff rate has been varied between $1.0{\cdot}10^{22}$ $s^{-1}$ and $3.0{\cdot}10^{22}$ $s^{-1}$. Ne seeding was not applied. The results are summarized in table 22.

Simulation results and conclusions are comparable to those for the scan in gas puff rate at zero ETB extension presented previously, as transport coefficients in the SOL and other simulation conditions are very similar. The far SOL transport coefficients

**Table 21.** Main plasma parameters achievable with and without extension of reduced transport to the SOL in an ITER D-T H-mode plasma at 15 MA / 5.3 T and 53 MW of additional power.

| Case | A | B | C | D |
|---|---|---|---|---|
| $P_{NBI}$ / $P_{ECRH}$ / $P_{ICRH}$ [MW] | 33 / - / 20 | 33 / - / 20 | 33 / - / 20 | 33 / 0 / 20 |
| $\Gamma_{D-T}$ [$10^{22}$ s$^{-1}$] / $\Gamma_{Ne}$ [$10^{20}$ s$^{-1}$] | 1.0 / - | 1.0 / - | 2.0 / - | 3.0 / - |
| $f_G$ | 0.67 | 0.50 | 0.73 | 0.82 |
| $n_e(0)$ / $< n_e >$ [$10^{19}$ m$^{-3}$] | 9.7 / 8.0 | 7.5 / 6.0 | 10.6 / 8.7 | 11.9 / 9.8 |
| $T_e(0)$ / $< T_e >$ [keV] | 19.0 / 9.9 | 21.0 / 11.8 | 18.0 / 9.3 | 17.1 / 8.6 |
| $T_i(0)$ / $< T_i >$ [keV] | 18.2 / 9.4 | 21.4 / 11.2 | 17.1 / 8.8 | 16.0 / 8.1 |
| $P_{fus}$ [MW] / $Q$ | 491.1 / 9.27 | 408.8 / 7.71 | 516.2 / 9.74 | 553.9 / 10.45 |
| Divertor material | W | W | W | W |
| $Z_{eff}$ | 1.01 | 1.01 | 1.01 | 1.01 |
| $P_{IT}$ / $P_{OT}$ [MW m$^{-2}$] | 21.5 / 15.0 | 11.0 / 14.8 | 10.0 / 14.0 | 12.0 / 9.0 |
| ETB extension in the SOL [mm] | 6.0 | 0.0 | 0.0 | 0.0 |

in the scan at zero ETB extension are the same as those applied everywhere in the SOL in this scan.

This scan provides an opportunity to do a closer comparison with predictions for similar ITER plasma configurations analysed in the past in simulations combining B2-EIRENE and ASTRA with the same SOL transport assumptions [17, 21]. In fact, the predictions for core fusion performance and the power crossing the separatrix from this simulation scan deviate only slightly from the simulations described in [17] (auxiliary power 53 MW and $< n_{D-T} >$ in the range 6-8·$10^{19}$ m$^{-3}$).

Indeed, more recent simulations with ASTRA including the self-consistent evaluation of the pedestal pressure from the EPED1 model and the SOL relations derived from B2-EIRENE in [17] found similar values of $Q$ for the densities modelled with JINTRAC [22]. In addition, the SOL parameter relation for the maximum power density at the target plates (including power deposited by radiation and neutral interaction) given in equations 1 and 4 in [17] seems to apply quite well also to the cases considered here. The neutral influx at the separatrix is estimated to be ∼1.0·$10^{21}$ s$^{-1}$ and in the same order of magnitude as that predicted by equation 5 in [17]. However, in absolute terms, the predicted main ion density at the separatrix is significantly higher in this scan than that given by equation 8 in [17]. According to equation 8, at the separatrix $n_{D-T} \approx 4.0 \cdot 10^{19}$ m$^{-3}$ for a power in the SOL of ∼120 MW, whereas $n_{D-T} \geq 5.0 \cdot 10^{19}$ m$^{-3}$ for this scan. It should be noted that from the point of view of divertor power load control, only the case at $\Gamma_{D-T} = 3.0 \cdot 10^{22}$ s$^{-1}$ is marginally compatible with the requirement of maintaining the peak divertor heat flux under 10 MW m$^{-2}$.

Because of the discrepancy in the separatrix density in absolute terms, the same fusion performance can be obtained in the JINTRAC calculations at much lower particle source rates with gas fuelling only, whereas in [17] some pellet fuelling had to be considered to achieve high core densities at limited densities at the separatrix. The differences in separatrix densities are related to the impurity species and concentrations considered in the two simulations (in this scan only Be and Ne were considered, whereas in the B2-EIRENE/ASTRA simulations the impurity mix

**Table 22.** Main plasma parameters achievable for different gas fuelling rates and transport in the SOL fixed as in [18] in an ITER D-T H-mode plasma at 15 MA / 5.3 T and 53 MW of additional power.

| Case | A | B | C |
|---|---|---|---|
| $P_{NBI}$ / $P_{ECRH}$ / $P_{ICRH}$ [MW] | 32 / - / 20 | 33 / - / 20 | 33 / - / 20 |
| $\Gamma_{D-T}$ [$10^{22}$ s$^{-1}$] / $\Gamma_{Ne}$ [$10^{20}$ s$^{-1}$] | 1.0 / - | 2.0 / - | 3.0 / - |
| $f_G$ | 0.50 | 0.73 | 0.84 |
| $n_e(0)$ / $< n_e >$ [$10^{19}$ m$^{-3}$] | 7.5 / 6.0 | 10.6 / 8.7 | 12.3 / 10.0 |
| $T_e(0)$ / $< T_e >$ [keV] | 21.0 / 11.8 | 18.0 / 9.3 | 17.0 / 8.6 |
| $T_i(0)$ / $< T_i >$ [keV] | 21.4 / 11.2 | 17.1 / 8.8 | 16.0 / 8.1 |
| $P_{fus}$ [MW] / $Q$ | 408.8 / 7.71 | 516.2 / 9.74 | 579.6 / 10.94 |
| Divertor material | W | W | W |
| $Z_{eff}$ | 1.01 | 1.01 | 1.01 |
| $P_{IT}$ / $P_{OT}$ [MW m$^{-2}$] | 11.0 / 14.9 | 10.4 / 14.1 | 12.1 / 10.2 |

included He, Be and C). Also the different assumptions for the material of plasma facing components (Be and W in this scan and C in the B2-EIRENE/ASTRA simulations) could have had some influence on the results. In fact, the impurity concentration in this scan ($Z_{eff} \leq 1.01$) is significantly lower compared to the simulations in [17] in which significant C sputtering is present and $Z_{eff} \geq 1.7$ at the separatrix for a power in the SOL ∼120 MW, according to equations 6, 8 and 11 in [17].

The increased impurity content in the simulations leads to an increase of the radiation in the SOL by ∼30-40 MW in the simulations in [17] compared to this scan, which leads to lower separatrix densities in the B2-EIRENE/ASTRA studies. Indeed, as already mentioned in [21] and in previous ITER edge modelling studies, simulations with low impurity content of ITER high $Q$ scenarios would require very high separatrix densities to achieve divertor power load control. These were considered not to be compatible with high pedestal pressure or high energy confinement required for high $Q$ in ITER on the assumption that the plasma behaviour observed in present experiments can be extrapolated to ITER, which as previously mentioned, remains to be proven.

Indeed, simulations with JINTRAC with Be divertor targets and low gas flux of $\Gamma_{D-T} = 0.75 \cdot 10^{22}$ s$^{-1}$ (not shown in this paper) have a higher $Z_{eff} \approx 1.7 - 1.8$, increased impurity radiation in the divertor and SOL and degraded fusion performance with a power in the SOL ∼95 MW. For such simulations, the main ion density at the separatrix dropped to lower values ∼ $2.5{\cdot}10^{19}$ m$^{-3}$, similar to those obtained for comparable conditions in [17]. Taking into account the discrepancies in impurity modelling assumptions, one can conclude that good overall agreement was found between independently performed JINTRAC and B2-EIRENE/ASTRA predictions for the 15 MA ITER baseline scenario core and edge Ne which strongly supports the validity of both of these integrated modelling approaches for stationary conditions.

### *6.11. Results at 15 MA / 5.3 T / 53 MW. Gas fuelling limits.*

To further investigate the limits of gas puff fuelling of a full field and current ITER ELMy H-mode plasma, we started from a simulation of a 15MA, 5.3T, 33MW NBI,

**Table 23.** Main plasma parameters achievable for different gas fuelling rates in an ITER D-T H-mode plasma at 15 MA / 5.3 T and 53 MW of additional power.

| Case | A | B |
|---|---|---|
| $P_{NBI}$ / $P_{ECRH}$ / $P_{ICRH}$ [MW] | 33 / - / 20 | 33 / - / 20 |
| $\Gamma_{D-T}$ [$10^{22}$ s$^{-1}$] / $\Gamma_{Ne}$ [$10^{20}$ s$^{-1}$] | 2.0 / - | 3.0 / - |
| $f_G$ | 0.80 | 0.90 |
| $n_e(0)$ / $< n_e >$ [$10^{19}$ m$^{-3}$] | 11.5 / 9.5 | 13.0 / 10.7 |
| $T_e(0)$ / $< T_e >$ [keV] | 21.9 / 11.2 | 21.2 / 10.4 |
| $T_i(0)$ / $< T_i >$ [keV] | 19.1 / 10.1 | 18.4 / 9.5 |
| $P_{fus}$ [MW] / $Q$ | 831.0 / 15.68 | 955.0 / 18.02 |
| Divertor material | W | W |
| $Z_{eff}$ | 1.00 | 1.00 |
| $P_{IT}$ / $P_{OT}$ [MW m$^{-2}$] | 13.8 / 31.1 | 13.7 / 30.2 |

20MW ICRH, $1.0{\cdot}10^{22}$ s$^{-1}$ gas puff rate simulation, with W and without impurity seeding. In three different runs we performed a gas rate scan by increasing the fuelling to $2.0{\cdot}10^{22}$ s$^{-1}$, $3.0{\cdot}10^{22}$ s$^{-1}$ and $4.0{\cdot}10^{22}$ s$^{-1}$ respectively.

The highest fuelling case $4.0{\cdot}10^{22}$ s$^{-1}$ reaches detachment rather soon, with the temperature at the divertor plate dropping below ∼1eV after ∼2 s. The results for the other two cases are summarized in table 23. For these lower gas rate cases the simulations show that, in theory, the volume average plasma density can be increased above $10^{20}$ m$^{-3}$, the on-axis ion temperature stabilizes at ∼20 keV resulting in a stable ELMy H-mode plasma with good confinement ($\alpha_c = 2$) and $P_{fus}$ in the range 0.8-1.0 GW.

These extremely optimistic values are a consequence of the fact that, according to these simulations, the density at the separatrix can be increased to values in the order of $8.0{\cdot}10^{19}$ m$^{-3}$ without degrading the confinement and without causing the detachment of the divertor. These assumptions are questionable because, experimentally, a degradation of the confinement is observed with increased gas rate and separatrix density and because without any impurity seeding the power load on the divertor plates exceeds the safe limit of 10 MW m$^{-2}$ in both cases and reaches 15 MW m$^{-2}$ on the inner divertor plate and 30 MW m$^{-2}$ on the outer divertor plate. Seeding is therefore mandatory in this scenario to keep the divertor power load below the limit required for safe operation. However, in presence of seeding, the divertor could detach for lower levels of gas puff and the density at the separatrix could reach lower values than in the simulations presented here.

## 7. Discussion

In the previous sections we have presented in detail simulations results for different fuelling, seeding and heating schemes for the flat-top of an ITER H-mode discharge at different plasma current and toroidal magnetic field.

The results show that, at 5 and 7.5 MA the fuelling of this phase of the discharge does not present particular problems. Densities above the limit required for safe operation of the beams avoiding shine-through can be maintained relatively easily by means of gas puff only and, because of the low fusion power generated in the plasma,

the control of the power density on the divertor plates does not represent a problem either. These conclusions are not critically sensitive to the hypothesis we made on the transport in the ETB and the SOL.

The situation changes radically when we increase the plasma current to 10 and 15 MA. For these levels of plasma current the requirements on the density are more challenging (especially if one wants to achieve a relatively high $Q$) and the increasing fusion power imposes an additional thermal load on the divertor.

As we have shown in the simulations presented in the previous sections the results depend crucially on the hypothesis made about the transport in the ETB and the SOL. In particular, if we assume that the transport is unaffected by the level of gas puff and the density at the separatrix is limited exclusively by the detachment of the divertor, we have shown that the required densities could be achieved by gas puff only. On the other hand, if we assume, as observed in present days experiments that gas puffing degrades the confinement and enhances the transport at the plasma edge, then gas puff alone might not be sufficient to achieve the density required to sustain $Q$=10.

In this case pellets will have to be used to fuel the discharge. Depending on the pellet mass, injection frequencies in the order of a few Hz are required. However, simulations show that, in certain conditions, too big pellets can cause perturbations of the separatrix density that can result in thermal instabilities and divertor detachment and threaten the stability of the discharge.

A further aspect highlighted by the simulations at plasma current above 10 MA is the power load on the divertor targets due to the fusion power generated inside the plasma. We have shown that, without any mitigation techniques, this can easily exceed the limit of 10 MW $m^{-2}$ considered acceptable for the safe operation of the ITER divertor. Moreover, the temperature in front of the divertor plates can exceed the limit of 5 eV, above which the sputtering of W by D becomes possible.

Our simulations show that a combination of a moderate rate of main gas puff and Ne seeding in the range $10^{19}$-$10^{20}$ $s^{-1}$ should be sufficient to maintain the power load on the divertor plates and the temperature in front of them below 10 MW $m^{-2}$ and 5 eV respectively, without endangering the thermal stability of the plasma, at least for this phase of the discharge. On this particular point, it is worth noting that our simulations indicate that Ne seeding alone seems to be insufficient to affect significantly the divertor thermal load and that will have to be used in combination with main gas puff.

Finally, we would like to point out that there are additional aspects (not considered in this study) that could affect the results presented in this paper. In particular, in a mitigated ELM regime (for example by resonant magnetic perturbations) the normalized pressure gradient in the ETB $\alpha_c$ could be lower than assumed in the simulations presented here, where the estimate of the pedestal pressure was based on unperturbed stability analysis. Moreover, in a mitigate ELM regime, one should expect a 'density pump-out' effect, which would likely affect the fuelling requirement for a given scenario [23]. The assessment of the impact of these phenomena on the simulations result is beyond the scope of this paper, since it is not clear at the moment how they could be included in the integrated scenario modelling.

## 8. Conclusions

In this paper we have analysed extensively the problem of fuelling the flat top of an ITER H-mode D-T plasma with particular attention to the possibility of attaining

densities compatible simultaneously with the safe operation of the NBI (avoiding the shine through, especially at low plasma current and density), the reduction of the power density load on the divertor plates to below 10 MW $m^{-2}$ and the achievement of fusion power in the order of 500 MW at 15 MA, resulting in $Q$=10. In doing so we have conducted several sensitivity studies aimed at assessing the less known aspects of the problem, in particular the detail of the transport in the ETB and the SOL.

The results of the analysis indicate that, in principle, it is possible to fuel the burn phase of an ITER H-mode D-T plasma at 15 MA and achieve $Q$=10 and, at the same time, maintain the power load on the divertor below 10 MW $m^{-2}$ by tuning the gas fuelling and the impurity seeding schemes to each particular scenario. The details of the fuelling, seeding and heating schemes to achieve these conditions have been described case by case. When simulations are performed in the same conditions, the results are in line with those of previous studies performed with different codes.

It should be noted that, in some circumstances, pellet fuelling will be necessary to achieve the required target density. In this case the transient perturbation induced by the pellet injection should be limited in size in order to avoid overloading the divertor with an excessive particle outflux and causing a thermal instability.

A detailed analysis of transient phenomena and of the phases leading to and out of a steady-state H-mode in ITER (namely current ramp-up including H-mode access and ramp-down including exit from the H-mode) will be the subject of further publications.

## Acknowledgments

JINTRAC was used under licence agreement between Euratom and CCFE, Ref. Ares(2014)3576010-28/10/2014. This work was funded jointly by the RCUK Energy Programme (grant number EP/I501045) and by ITER Task Agreement C19TD51FE implemented by Fusion for Energy under Grant GRT-502. To obtain further information on the data and models underlying this paper, whose release may be subject to commercial restrictions, please contact PublicationsManager@ukaea.uk. The views and opinions expressed do not necessarily reflect those of Fusion for Energy which is not liable for any use that may be made of the information contained herein. The views and opinions expressed herein do not necessarily reflect those of the ITER Organization.

## References

[1] M Romanelli, V Parail, P da Silva Aresta Belo, G Corrigan, L Garzotti, D Harting, F Koechl, E Militello-Asp, R Ambrosino, M Cavinato, A Kukushkin, A Loarte, M Mattei and R Sartori 2015 *Nucl. Fusion* **55** 093008

[2] E Militello Asp, G Corrigan, P da Silva Arresta Belo, L Garzotti, D Harting, F Koechl, V Parail, M Cavinato, A Loarte, M Romanelli and R Sartori, 2017, *26th IAEA Fusion Energy Conference (Kyoto, Japan 17 - 22 October 2016)*, eds R. Kaiser, S. M. González de Vicente, R. Kamendje (Vienna: International Atomic Energy Agency) TH/P2-23

[3] Romanelli M, Corrigan G, Parail V, Wiesen S, Ambrosino R, Da Silva Aresta Belo P, Garzotti L, Harting D, Köchl F, Koskela T, Lauro-Taroni L, Marchetto C, Mattei M, Militello-Asp E, Nave M F F, Pamela S, Salmi A, Starnd P, Szepesi G and EFDA-JET Contributors 2014 *Plasma and Fusion Research* **9** 3403023

[4] Houlberg W A, Shaing K C, Hirshman S P, Zarnstorff M C, 1997 *Phys. Plasmas* **4** 3230

[5] Erba M, Cherubini A, Parail V V, Springmann E and Taroni A 1997 *Plasma Phys. Control. Fusion* **39** 261

[6] Waltz R E, Staebler G M, Dorland W, Hammett G W, Kotschenreuther K and Konings J A 1997 *Phys. Plasmas* **4** 2482
[7] Parail V, Belo P, Boerner P, Bonnin X, Corrigan G, Coster D, Ferreira J, Foster A, Garzotti L, Hogeweij G M D, Houlberg W, Imbeaux F, Johner J, Köchl F, Kotov V, Lauro-Taroni L, Litaudon X, Lonnroth J, Pereverzev G, Peysson Y, Saibene G, Sartori R, Schneider M, Sips G, Strand P, Tardini G, Valovič M, Wiesen S, Wischmeier M, Zagórski R, JET EFDA contributors and EU ITM Task Force 2009 *Nucl. Fusion* **49** 075030
[8] Snyder P B, Groebner R J, Hughes J W, Osborne T H, Beurskens M, Leonard A W, Wilson H R and Xu X Q 2011 *Nucl. Fusion* **51** 103016
[9] M Groth, G D Porter, T D Rognlien, S Wiesen, M Wischmeier, M N A Beurskens, X Bonnin, B D Bray, S Brezinsek, N H Brooks, D P Coster, T Eich, M E Fenstermacher, C Fuchs, R A Groebner, D Harting, A Huber, S Jachmich, A Kallenbach, C J Lasnier, A W Leonard, A Meigs, H W Mller, M E Rensink, D L Rudakov, J G Watkins, E Wolfrum, the DIII-D and ASDEX Upgrade Teams and JET EFDA Contributors 2011 *Plasma Phys. Control. Fusion* **53** 124017
[10] S Wiesen, W Fundamenski, M Wischmeier, M Groth, S Brezinsek, V Naulin and JET EFDA contributors 2010 *J. Nuc. Mat.* **415** S535
[11] Belo P, Romanelli M, Parail V, Corrigan G, Harting D, Garzotti L, Köchl F, Militello-Asp E, Mattei M, Ambrosino R, Loarte A, Kukushkin A S, Sartori R, Cavinato M, 2015 *42$^{th}$ European Physical Society Conf. on Plasma Physics (Lisbon, Portugal, 22 - 26 June 2015)* vol **39E** (Europhysics Conference Abstracts) eds Bingham R, Suttrop W, Atzeni S, Foest R, McClements K (Mulhouse: European Physical Society) P4.120
[12] Challis C D, Cordey J G, Hamnen H, Stubberfield P M, Christiansen J P, Lazzaro E, Muir D G, Stork D and Thompson E 1989 *Nucl. Fusion* **29** 563
[13] Reiter D, Baelmans M and Börner P 2005 *Fus. Sc. Tech.* **47** 172 and online documentation at www.eirene.de
[14] Pégourié B, Waller V, Nehme H, Garzotti L and Géraud A 2007 *Nucl. Fusion* **47** 44
[15] P Maget, J-F Artaud, M Bécoulet, T Casper, J Faustin, J Garcia, G T A Huijsmans, A Loarte and G Saibene 2013 *Nucl. Fusion* **53** 093011
[16] T Eich, A W Leonard, R A Pitts, W Fundamenski, R J Goldston, T K Gray, A Herrmann, A Kirk, A Kallenbach, O Kardaun, A S Kukushkin, B LaBombard, R Maingi, M A Makowski, A Scarabosio, B Sieglin, J Terry, A Thornton, ASDEX Upgrade Team and JET EFDA Contributors 2013 *Nucl. Fusion* **53** 093031
[17] H D Pacher, A S Kukushkin, G W Pacher, V Kotov and D Reiter 2011 *J. Nuc. Mat.* **415** S492
[18] A S Kukushkin, H D Pacher, G W Pacher, V Kotov, R A Pitts and D Reiter 2013 *J. Nuc. Mat.* **438** S203
[19] Garzotti L, Belo P, Corrigan G, Köchl F, Lönnroth J, Parail V, Pereverzev G, Saarelma S, Tardini G, Valovič M 2012 *Nucl. Fusion* **52** 013002
[20] O. Sauter, C. Angioni and Y. R. Lin-Liu 1999 *Phys. Plasmas* **6** 2839
[21] G W Pacher, H D Pacher, G Janeschitz and A S Kukushkin 2008 *Nucl. Fusion* **48** 105003
[22] A R Polevoi, A Loarte, N Hayashi, H S Kim, S H Kim, F Koechl, A S Kukushkin, V M Leonov, S Yu Medvedev, M Murakami, Y S Na, A Y Pankin, J M Park, P B Snyder, J A Snipes, V E Zhogolev, the IOS ITPA TG 2015 *Nucl. Fusion* **55** 063019
[23] M Valovič, P T Lang, A Kirk, W Suttrop, M Cavedon, G Cseh, M Dunne, L R Fischer, L Garzotti, L Guimarais, G Kocsis, A Mlynek, B Plöckl, R Scannell, T Szepesi, G Tardini, A Thornton, E Viezzer, E Wolfrum, the ASDEX Upgrade Team and the EUROfusion MST Team 2016 *Nucl. Fusion* **56** 066009

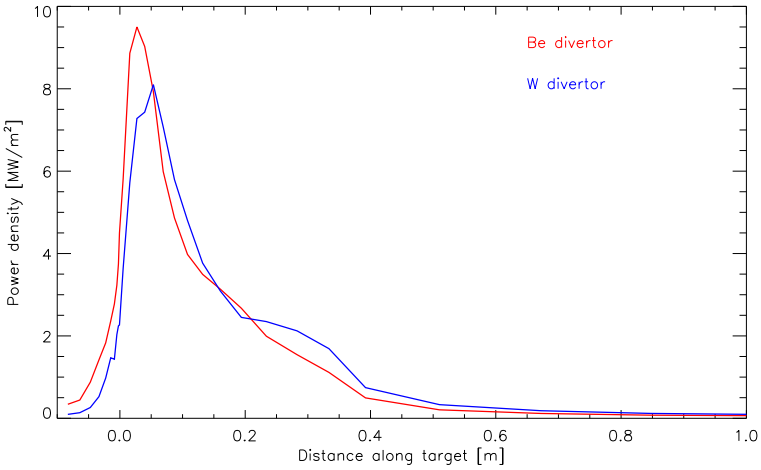


**Figure 1.** Outer target power density profile for case C in table 10 (red) and case D in table 11 (blue).

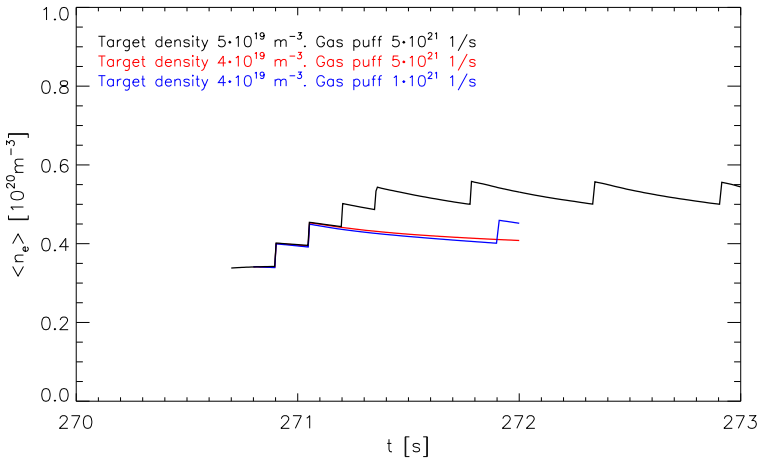


**Figure 2.** Evolution and control of the plasma volume-average density by means of pellet injection in 7.5 MA / 2.65 T ITER D-T baseline H-mode with 33 MW of NB for different target volume-average densities and with different levels of back ground gas puff. The target densities are easily achieved and maintained.

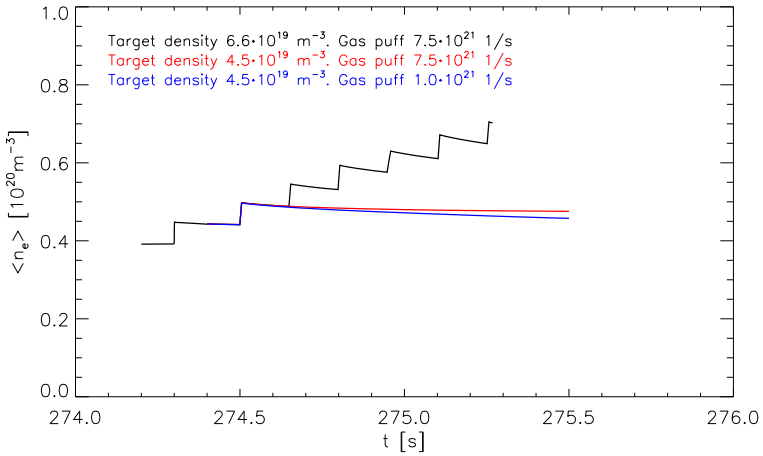


**Figure 3.** Evolution and control of the plasma volume-average density by means of pellet injection in 10 MA / 5.3 T ITER D-T baseline H-mode with 33 MW of NB and 20 MW of ICRH for different target volume-average densities and with different levels of back ground gas puff. The target densities are easily achieved and maintained.

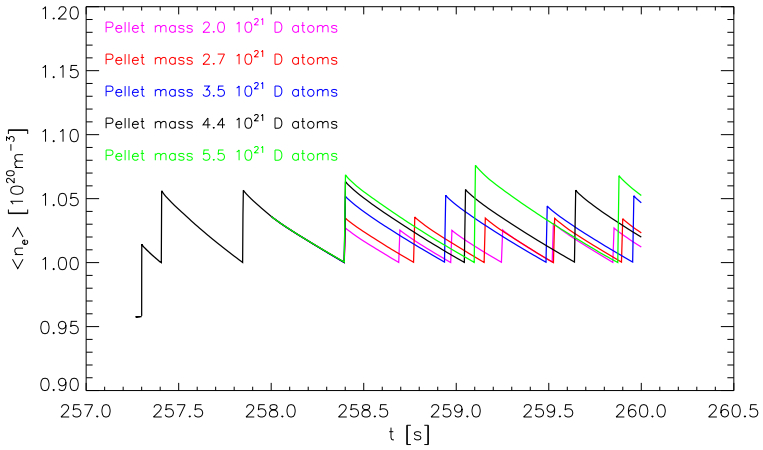


**Figure 4.** Evolution and control of the plasma volume-average density by means of pellet injection in 15 MA / 5.3 T ITER D-T baseline H-mode with 33 MW of NB and 20 MW of ICRH for a target volume-average density of $10^{20}$ m$^{-3}$ and with different levels of back ground gas puff. The target densities are easily achieved and maintained.

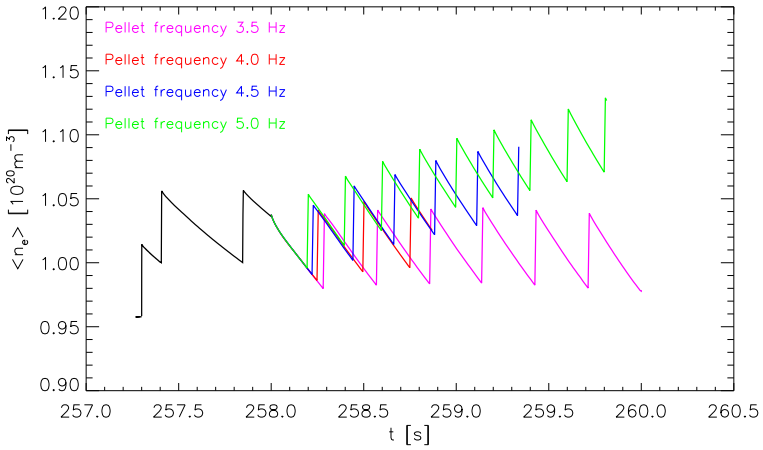


**Figure 5.** Evolution of the plasma volume-average density by means of pellet injection in 15 MA / 5.3 T ITER DT baseline H-mode with 33 MW of NB and 20 MW of ICRH for different fixed pellet frequencies.

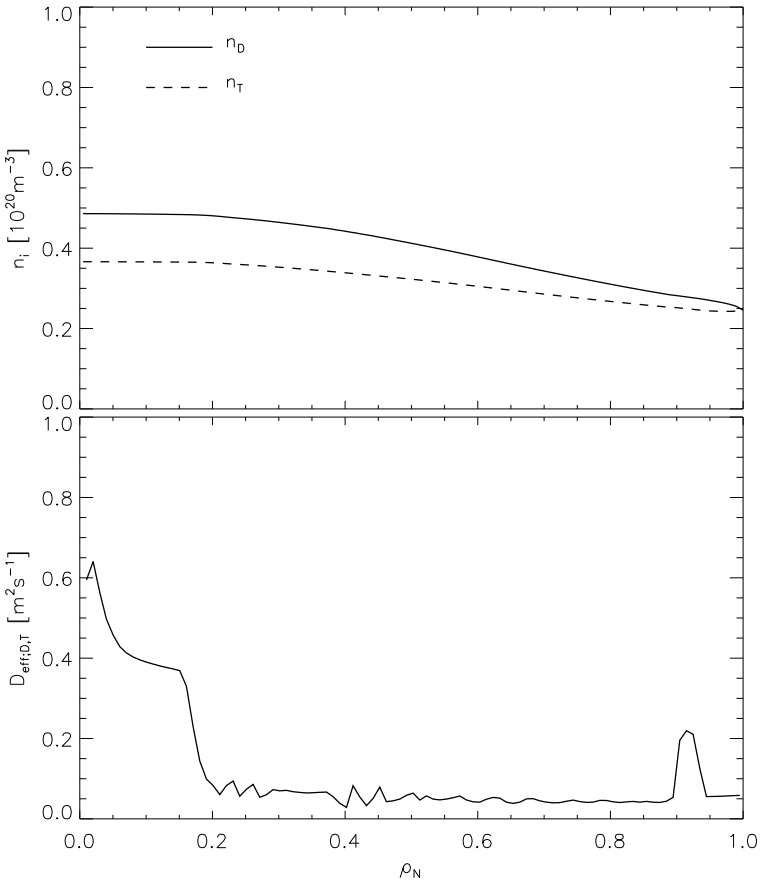


**Figure 6.** D and T density and effective diffusivity profiles for a JETTO-SANCO core transport simulation with GLF23 and NCLASS taking into account momentum transport of an ITER D-T H-mode plasma at 15 MA / 5.3 T with 33MW of NB and 20MW of ICRH, W targets, in steady-state conditions. (Table 16 case A).

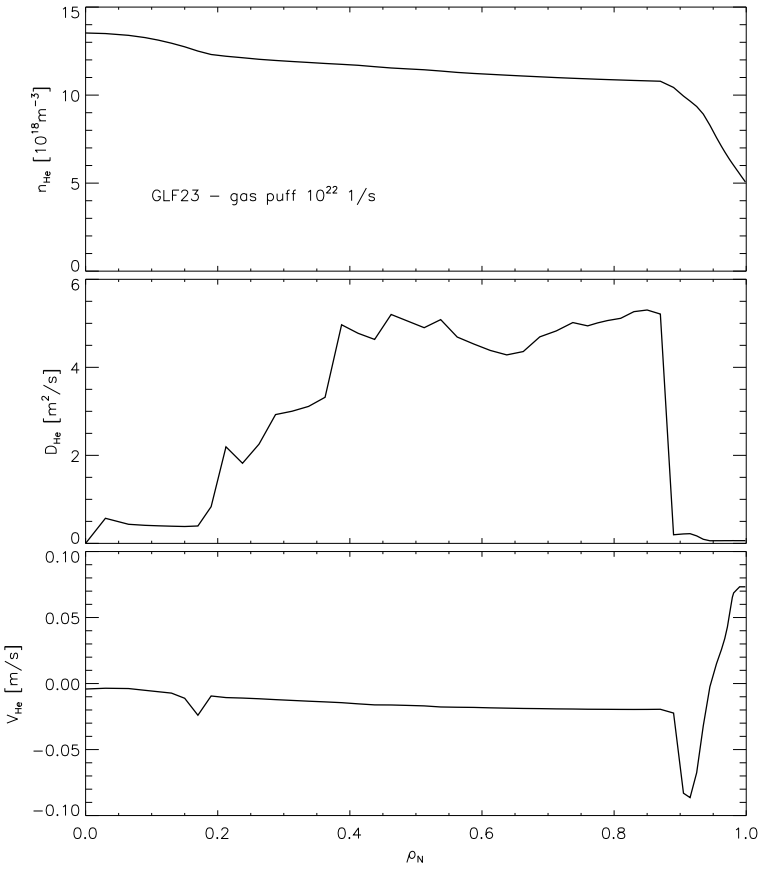


**Figure 7.** He density, He diffusivity and He convective velocity profiles for a JETTO-SANCO core transport simulation with GLF23 and NCLASS taking into account momentum transport of an ITER D-T H-mode plasma at 15 MA / 5.3 T with 33MW of NB and 20MW of ICRH, W targets, in steady-state conditions. (Table 16 case A).

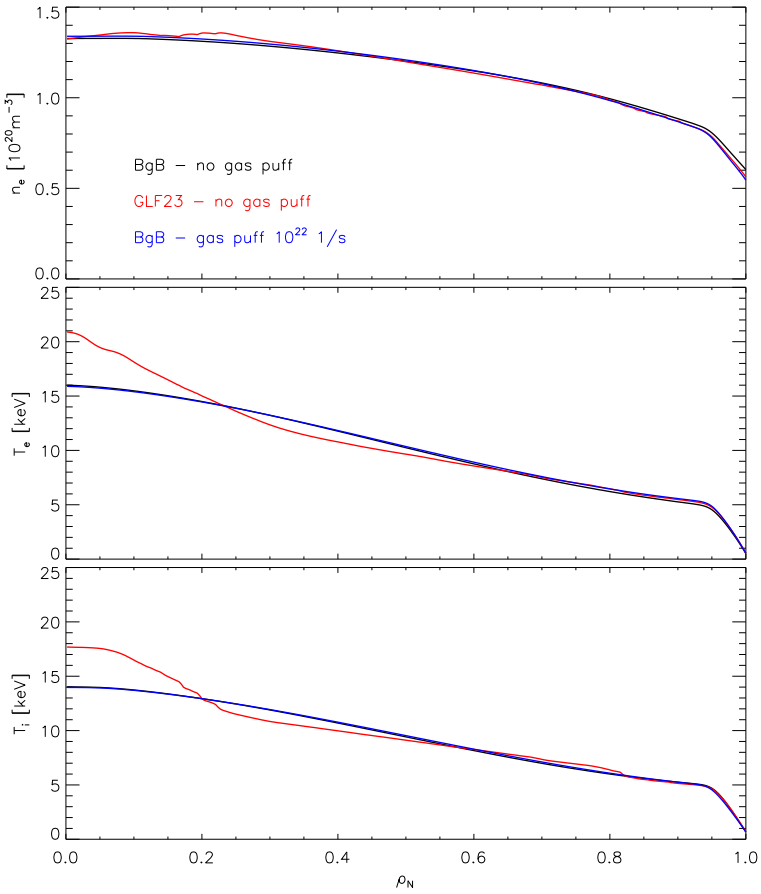


**Figure 8.** Comparison of electron density and temperature profiles for a quasi-stationary pellet fuelled burning H-mode plasma at 15 MA / 5.3 T, with 33 MW of NB and 20 MW of ICRH and $Q \approx 10$ with core transport modelled with either the GLF23-like Bohm/gyro-Bohm model (red) or the GLF23 model (blue). In these cases there is no D-T gas puff and Ne radiation in the SOL amounts to a few MW only. A third case with $\Gamma_{D-T} = 10^{22}$ s$^{-1}$ is also shown for comparison.

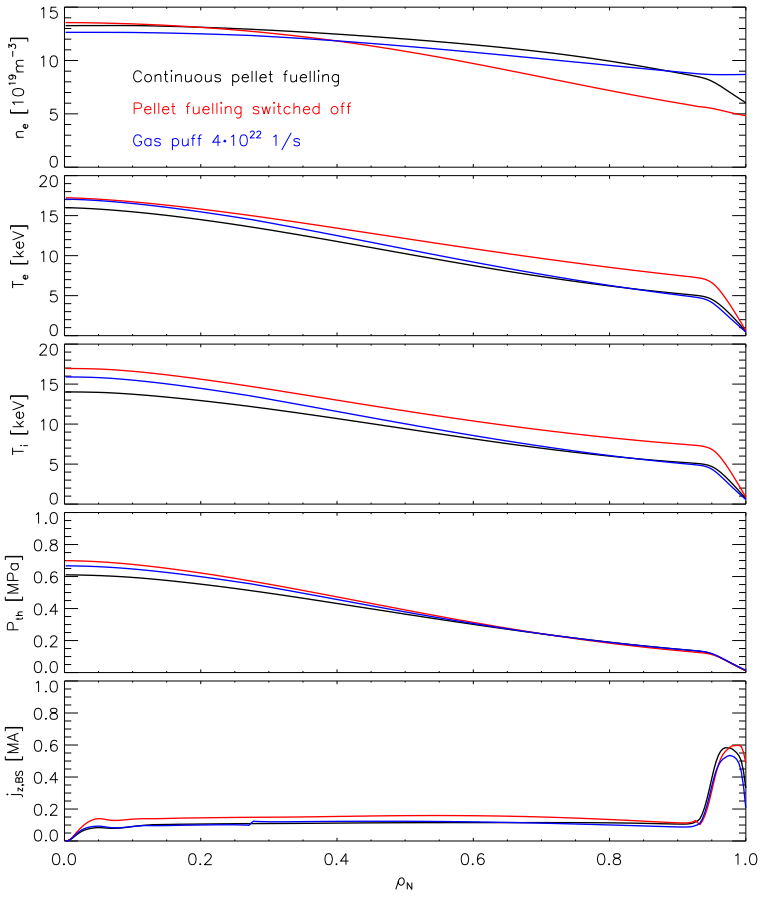


**Figure 9.** Electron density, electron temperature, ion temperature, thermal pressure and toroidal bootstrap current density profiles for three DT H-mode plasma simulations at 15 MA / 5.3 T, $P_{aux}$ = 53 MW with W targets with pellet fuelling (red), with density decaying from stationary conditions with pellet fuelling to those with gas fuelling at low puff rates (green) and with strong gas fuelling ($\Gamma_{D-T} = 4 \cdot 10^{22}$ s$^{-1}$).

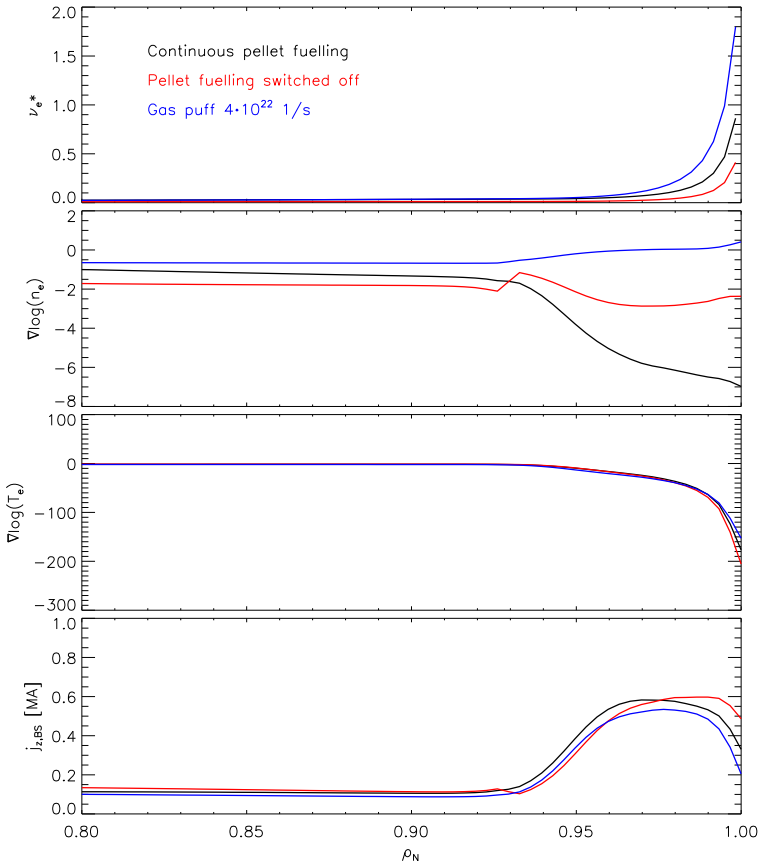


**Figure 10.** Profiles in the plasma edge region of normalized electron collisionality, logarithmic electron density derivative, logarithmic electron temperature derivative and bootstrap current density for three D-T H-mode plasma simulations at at 15 MA / 5.3 T, $P_{aux}$ = 53 MW with W targets with pellet fuelling (red), with density decaying from stationary conditions with pellet fuelling to those for gas fuelling at low gas fuelling rates (green) and with strong gas fuelling ($\Gamma_{D-T} = 4 \cdot 10^{22}$ s$^{-1}$).